

 Open access • Posted Content • DOI:10.21203/RS.3.RS-235272/V1

COVA1-18 neutralizing antibody protects against SARS-CoV-2 in three preclinical models. — [Source link](#)

[Roger Le Grand](#), [Pauline Maisonnasse](#), [Yoann Aldon](#), [Aurélien Marc](#) ...+46 more authors

Institutions: [Université Paris-Saclay](#), [University of Amsterdam](#), [University of Paris](#), [University of Texas Medical Branch](#) ...+3 more institutions

Published on: 15 Feb 2021

Topics: [Neutralizing antibody](#) and [Viral load](#)

Related papers:

- [Naturally enhanced neutralizing breadth to SARS-CoV-2 after one year](#)
- [Eicosanoid signaling as a therapeutic target in middle-aged mice with severe COVID-19](#)
- [A highly potent antibody effective against SARS-CoV-2 variants of concern.](#)
- [SARS -CoV-2 T-cell immunity to variants of concern following vaccination](#)
- [Live imaging of SARS-CoV-2 infection in mice reveals neutralizing antibodies require Fc function for optimal efficacy](#)

Share this paper:    

View more about this paper here: <https://typeset.io/papers/cova1-18-neutralizing-antibody-protects-against-sars-cov-2-52hi9oi8qt>

COVA1-18 neutralizing antibody protects against SARS-CoV-2 in three preclinical models

Pauline Maisonnasse

CEA - Université Paris Saclay - INSERM U1184 <https://orcid.org/0000-0002-0555-207X>

Yoann Aldon

Amsterdam UMC

Aurélien Marc

INSERM

Romain Marlin

CEA <https://orcid.org/0000-0001-8932-0171>

Nathalie Dereuddre-Bosquet

CEA <https://orcid.org/0000-0001-6682-6313>

Natalia Kuzmina

University of Texas <https://orcid.org/0000-0001-6650-9369>

Alec Freyn

Icahn School of Medicine at Mount Sinai

Jonne Snitselaar

Amsterdam UMC

Antonio Gonçalves

Université de Paris / INSERM <https://orcid.org/0000-0002-8759-2429>

Tom Caniels

Department of Medical Microbiology, Amsterdam UMC, University of Amsterdam, Amsterdam Infection & Immunity Institute, Amsterdam, the Netherlands <https://orcid.org/0000-0001-9580-157X>

Judith Burger

Amsterdam UMC

Meliawati Poniman

Amsterdam UMC

Virginie Chesnais

Life&Soft

Ségolène Diry

Life&Soft

Anton Iershov

Life&Soft

Adam Ronk

University of Texas

Sonia Jangra

Icahn School of Medicine at Mount Sinai

Raveen Rathnasinghe

Icahn School of Medicine at Mount Sinai

Philip Brouwer

Department of Medical Microbiology, Amsterdam UMC, University of Amsterdam, Amsterdam Infection & Immunity Institute, Amsterdam, the Netherlands

Tom Bijl

Amsterdam UMC

Jelle van Schooten

Amsterdam UMC <https://orcid.org/0000-0002-5202-355X>

Mitch Brinkkemper

Amsterdam UMC

Hejun Liu

The Scripps Research Institute

Meng Yuan

The Scripps Research Institute <https://orcid.org/0000-0001-9754-4503>

Chad Mire

The University of Texas Medical Branch at Galveston <https://orcid.org/0000-0001-7596-1808>

Mariëlle van Breemen

Amsterdam UMC

Vanessa Contreras

CEA - Université Paris Saclay - INSERM U1184

Thibaut Naninck

CEA – Université Paris Saclay – INSERM U1184

Julien Lemaitre

CEA – Université Paris Saclay – INSERM U1184

Nidhal Kahlaoui

Université Paris-Saclay, Inserm, CEA, Center for Immunology of Viral, Auto-immune, Hematological and Bacterial diseases

Francis Relouzat

CEA

Catherine Chapon

CEA – Université Paris Saclay – INSERM U1184

Raphael Ho Tsong Fang

CEA – Université Paris Saclay – INSERM U1184

Charlene McDanal

Duke University

Mary Osei-Twum

Nexelis

Natalie St-Amant

Nexelis

Luc Gagnon

Nexelis

David Montefiori

Duke University

Ian Wilson

Scripps Research Institute <https://orcid.org/0000-0002-6469-2419>

Eric Ginoux

Life&Soft

Godelieve de Bree

Department of Internal Medicine, Amsterdam UMC, University of Amsterdam, Amsterdam Infection & Immunity Institute, 1105AZ Amsterdam, the Netherlands

Adolfo Garcia-Sastre

Icahn School of Medicine at Mount Sinai <https://orcid.org/0000-0002-6551-1827>

Michael Schotsaert

Icahn School of Medicine at Mount Sinai <https://orcid.org/0000-0003-3156-3132>

Lynda Coughlan

University of Maryland School of Medicine <https://orcid.org/0000-0001-9880-6560>

Alexander Bukreyev

The University of Texas Medical Branch at Galveston <https://orcid.org/0000-0002-0342-4824>

Sylvie van der Werf

Institut Pasteur <https://orcid.org/0000-0002-1148-4456>

Jeremie Guedj

INSERM <https://orcid.org/0000-0002-5534-5482>

Rogier Sanders

Department of Medical Microbiology, Amsterdam UMC, University of Amsterdam, Amsterdam Infection & Immunity Institute, Amsterdam, the Netherlands

Marit van Gils

Amsterdam UMC, University of Amsterdam

Roger Le Grand (✉ roger.le-grand@cea.fr)

Université Paris-Saclay, INSERM, CEA <https://orcid.org/0000-0002-4928-4484>

Biological Sciences - Article

Keywords: COVID-19, SARS-CoV-2, COVA1-18, monoclonal antibodies

Posted Date: February 15th, 2021

DOI: <https://doi.org/10.21203/rs.3.rs-235272/v1>

License:  This work is licensed under a Creative Commons Attribution 4.0 International License.

[Read Full License](#)

Version of Record: A version of this preprint was published at Nature Communications on October 20th, 2021. See the published version at <https://doi.org/10.1038/s41467-021-26354-0>.

1 COVA1-18 neutralizing antibody protects against SARS-CoV-2 in three 2 preclinical models

3
4 Maisonnasse, P^{1*}; Aldon, Y^{2*}; Marc, A³; Marlin, R¹; Dereuddre-Bosquet, N¹; Kuzmina, NA^{4,5};
5 Freyn, AW⁶; Snitselaar, JL²; Gonçalves, A³; Caniels, TG²; Burger, JA²; Poniman, M²;
6 Chesnais, V⁷; Diry, S⁷; Iershov, A⁷; Ronk, AJ^{4,5}; Jangra, S⁶; Rathnasinghe, R^{6,8}; Brouwer,
7 PJM²; Bijl, TPL²; van Schooten, J²; Brinkkemper, M²; Liu, H⁹; Yuan, M⁹; Mire, CE^{5,10}; van
8 Breemen, MJ²; Contreras V¹; Naninck T¹; Lemaître, J¹; Kahlaoui, N¹; Relouzat, F¹; Chapon,
9 C¹; Ho Tsong Fang, R¹; McDanal, C¹¹; Osei-Twum, M¹²; St-Amant, N¹²; Gagnon, L¹²;
10 Montefiori, DC¹¹; Wilson, IA⁹; Ginoux, E⁷; de Bree, GJ¹³; García-Sastre, A^{6,14,15,16}; Schotsaert,
11 M^{6,16}; Coughlan, L^{6,17}; Bukreyev, A^{4,5,10}; van der Werf, S^{18,19}; Guedj, J³; Sanders, RW^{2,20}; van
12 Gils, MJ²; Le Grand, R¹

13 14 **Affiliations:**

15 ¹ Université Paris-Saclay, Inserm, CEA, Center for Immunology of Viral, Auto-immune,
16 Hematological and Bacterial diseases (IMVA-HB/IDMIT), Fontenay-aux-Roses & Le
17 Kremlin-Bicêtre, Paris, France.

18 ² Departments of Medical Microbiology of the Amsterdam UMC, University of Amsterdam,
19 Amsterdam Institute for Infection and Immunity, 1105 AZ, Amsterdam, The Netherlands.

20 ³ Université de Paris, INSERM, IAME, F-75018 Paris, France.

21 ⁴ Department of Pathology, University of Texas Medical Branch at Galveston, Texas, USA

22 ⁵ Galveston National Laboratory, Texas, USA.

23 ⁶ Department of Microbiology, Icahn School of Medicine at Mount Sinai, New York (NY),
24 USA.

25 ⁷ Life and Soft, 92350 Le Plessis-Robinson, France.

26 ⁸ Graduate School of Biomedical Sciences, Icahn School of Medicine at Mount Sinai, New
27 York (NY), USA.

28 ⁹ Department of Integrative Structural and Computational Biology, The Scripps Research
29 Institute, La Jolla, CA 92037, USA.

30 ¹⁰ Department of Microbiology, University of Texas Medical Branch at Galveston, Texas,
31 USA.

32 ¹¹ Duke Human Vaccine Institute & Department of Surgery, Durham, NC 27710, USA.

33 ¹² Nexelis, Laval, Québec, Canada.

34 ¹³ Internal Medicine of the Amsterdam UMC, University of Amsterdam, Amsterdam Institute
35 for Infection and Immunity, 1105 AZ, Amsterdam, The Netherlands.

36 ¹⁴ Department of Medicine, Division of Infectious Diseases, Icahn School of Medicine at
37 Mount Sinai, New York (NY), USA.

38 ¹⁵ The Tisch Cancer Institute, Icahn School of Medicine at Mount Sinai, New York (NY),
39 USA.

40 ¹⁶ Global Health and Emerging Pathogens Institute, Icahn School of Medicine at Mount
41 Sinai, New York (NY), USA.

42 ¹⁷ University of Maryland School of Medicine, Department of Microbiology and Immunology
43 and Center for Vaccine Development and Global Health (CVD), 685 W. Baltimore Street,
44 HSF1, Office #380E, Baltimore, MD 21201.

45 ¹⁸ Molecular Genetics of RNA Viruses, Department of Virology, Institut Pasteur, CNRS
46 UMR 3569, Université de Paris, Paris, France.

47 ¹⁹ National Reference Center for Respiratory Viruses, Institut Pasteur, Paris, France.

48 ²⁰ Department of Microbiology and Immunology, Weill Medical College of Cornell
49 University, New York, NY 10021, USA.

50

51 * These authors contributed equally.

52

53 **Abstract**

54 One year into the Coronavirus Disease 2019 (COVID-19) pandemic caused by Severe Acute
55 Respiratory Syndrome coronavirus 2 (SARS-CoV-2), effective treatments are still needed¹⁻³.
56 Monoclonal antibodies, given alone or as part of a therapeutic cocktail, have shown promising
57 results in patients, raising the hope that they could play an important role in preventing clinical
58 deterioration in severely ill or in exposed, high risk individuals⁴⁻⁶. Here, we evaluated the
59 prophylactic and therapeutic effect of COVA1-18 *in vivo*, a neutralizing antibody isolated from
60 a convalescent patient⁷ and highly potent against the B.1.1.7. isolate^{8,9}. In both prophylactic
61 and therapeutic settings, SARS-CoV-2 remained undetectable in the lungs of COVA1-18
62 treated hACE2 mice. Therapeutic treatment also caused a dramatic reduction in viral loads in
63 the lungs of Syrian hamsters. When administered at 10 mg kg⁻¹ one day prior to a high dose
64 SARS-CoV-2 challenge in cynomolgus macaques, COVA1-18 had a very strong antiviral
65 activity in the upper respiratory compartments with an estimated reduction in viral infectivity
66 of more than 95%, and prevented lymphopenia and extensive lung lesions. Modelling and
67 experimental findings demonstrate that COVA1-18 has a strong antiviral activity in three
68 different preclinical models and could be a valuable candidate for further clinical evaluation.

69 **Main text**

70 Across the world, the Coronavirus Disease 19 (COVID-19) pandemic caused by severe acute
71 respiratory syndrome coronavirus 2 (SARS-CoV-2) continues to escalate¹⁰. Despite the
72 progressive rollout of vaccines, there remains an urgent need for both curative and preventive
73 measures, especially in individuals with high risk. Monoclonal neutralizing antibodies (NABs),
74 isolated from convalescent COVID-19 patients, are one of the most promising approaches and
75 two NAb-based products have already received an emergency use authorization by the FDA.
76 Although their clinical efficacy remains to be fully assessed⁴⁻⁶, their capability to reduce viral
77 loads^{4,5} shows sufficient promise that such an approach could be effective if the treatment is
78 administered early enough.

79

80 We and others have previously isolated and characterized several highly potent monoclonal
81 NABs with half-maximum inhibitory concentration (IC₅₀) values in the picomolar range^{7,11-14},
82 with the majority of these targeting the receptor binding domain (RBD) on the S1 subunit of
83 the S protein. We previously identified COVA1-18, an RBD-specific monoclonal Ab, as one
84 of the most potent NAB *in vivo*⁷. Using three different experimental models as well as
85 mathematical modeling, we demonstrate that its rapid and extensive biodistribution is
86 associated with a very potent antiviral effect, and make it a promising candidate for clinical
87 evaluation, both as a prophylactic or therapeutic treatment of COVID-19.

88

89 **COVA1-18 *in vitro* potency is dependent on avidity**

90 To advance our earlier *in vitro* results⁷ on COVA1-18 and allow for better comparability with
91 other studies, we used two new pseudovirus assays, one using lentiviral pseudotypes with an
92 ACE2-expressing 293T cell line¹⁵, and one using VSV-pseudotypes with Vero E6 cells¹⁶, to
93 confirm the potency of COVA1-18. With these assays, we confirmed the remarkable potency
94 of COVA1-18 IgG which inhibited lentiviral SARS-CoV-2 pseudovirus with an IC₅₀ of 0.8 ng
95 ml⁻¹ (5.2 pM) and VSV-based pseudovirus with an IC₅₀ of 9 ng ml⁻¹ (60 pM) (**Extended Data**
96 **Fig. 1a, Extended Data Table 1**). These results were corroborated in multiple independent labs
97 and COVA1-18 was also equipotent against the D614G variant (**Extended Data Table 1**) that
98 now dominates worldwide¹⁷⁻²¹ as well as the recently emerged B.1.1.7 variant that includes the
99 N501Y mutation^{8,9}.

100

101 COVA1-18 bound strongly to SARS-CoV-2 S protein and showed no cross-reactivity with S
102 proteins of SARS-CoV, MERS-CoV and common cold coronaviruses HKU1-CoV, 229E-CoV
103 and NL63-CoV (Extended Data Fig. 1b)⁷. Biolayer interferometry experiments showed that
104 COVA1-18 IgG bound to soluble SARS-CoV-2 S protein with an apparent dissociation
105 constant (K_D) of 5 nM, and its affinity for RBD was similar at 7 nM (Fig. 1a, Extended Data
106 Fig. 1c, d, Extended Data Table 1). Its Fab displayed a 12-fold weaker binding to RBD
107 compared to IgG (84 nM), with the difference mainly caused by a faster Fab off-rate (Fig. 1a,
108 Extended Data Table 1), also observed in a different assay setting (Extended Data Fig. 1d).
109 With an IC_{50} of 199 ng ml⁻¹, the COVA1-18 Fab was 237-fold less potent at neutralizing SARS-
110 CoV-2 pseudovirus, showing that the IgG avidity effect is important for COVA1-18
111 neutralization potency (Extended Data Fig. 1a, Extended Data Table 1).

112

113 **COVA1-18 inhibits viral replication in rodents**

114 We sought to evaluate whether COVA1-18 could control SARS-CoV-2 viral infection in a
115 previously described Ad5-hACE2 mouse model^{22,23} using a 10 mg kg⁻¹ dose. COVA1-18
116 administered intraperitoneally 24 h prior to, or after a SARS-CoV-2 challenge with 10⁴ plaque
117 forming units (PFU) was fully protective with no detectable viral replication in the lungs (Fig.
118 1b, c). We then tested the efficacy of COVA1-18 in the golden Syrian hamster model (n = 5
119 per group), which is naturally susceptible to SARS-CoV-2 and develop severe pneumonia upon
120 infection²⁴. We evaluated the effect on lung viral loads of 10 mg kg⁻¹ of COVA1-18 given 24
121 h after a 10⁵ PFU intranasal challenge (Fig. 1b, d). At 3 days post-infection (d.p.i.), 3/5 animals
122 had high serum neutralization while 2/5 animals had low neutralization activity (Extended Data
123 Fig. 1e). On day 3, the COVA1-18 treated group had significantly lower median lung viral
124 titers compared to the control group (3.5 vs 6.7 log₁₀ PFU g⁻¹, respectively, $p < 0.01$) with lowest
125 viral titers in the higher serum neutralizers (Fig. 1d).

126

127 **COVA1-18 PrEP prevents infection in NHP**

128 We evaluated the potential of COVA1-18 to prevent SARS-CoV-2 infection in cynomolgus
129 macaques in a pre-exposure prophylaxis (PrEP) study. The animals were treated intravenously
130 24 h prior to viral challenge with a dose of 10 mg kg⁻¹ of COVA1-18 (Fig. 2a). Treated and
131 control animals (n = 5 per group) were challenged on day 0 with 10⁶ PFU of SARS-CoV-2 via
132 combined intranasal and intratracheal routes using an experimental protocol developed
133 previously^{25,26}. On the day of challenge, the mean COVA1-18 serum concentration was 109 ±
134 2.7 µg ml⁻¹ (Fig. 2b, Extended Data Fig. 2a), and 4/5 animals had serum neutralization activity

135 while no neutralization activity was observed in the control group (Extended Data Fig. 2b-d).
136 COVA-18 was also detected in all respiratory tract samples and rectal samples (Fig. 2c-e,
137 Extended Data Fig. 3a-c), and represented on average 1.5% and 1.2% of the total IgG in heat-
138 inactivated content in the nasopharyngeal and tracheal mucosae, respectively. These levels
139 remained constant throughout the study period and similar levels were detected at 3 d.p.i. in
140 bronchoalveolar lavages (BAL) and saliva (Fig. 2e-f). As SARS-CoV-2 can cause damage to
141 non-respiratory organs, we performed a pharmacokinetic study on two additional macaques to
142 characterize the COVA1-18 distribution within the first 24 h (Extended Data Fig. 3d-f).
143 COVA1-18 was found in all organs studied, including the lungs, at concentrations of 4 to 22
144 ng mg⁻¹ of tissue, except for the brain where concentrations were substantially lower (250 pg
145 mg⁻¹ of tissue). Altogether, these data showed that COVA1-18 administered intravenously was
146 rapidly and efficiently distributed to the natural sites of infection as well as to organs affected
147 by COVID-19 pathology.

148

149 Following viral challenge, control animals showed similar genomic (g)RNA and subgenomic
150 (sg)RNA levels and kinetics as previously described^{25,26} with median peak viral loads (VL) of
151 6.4 and 6.2 log₁₀ copies per ml at 1-2 d.p.i. in the nasopharyngeal and tracheal swabs,
152 respectively (Fig. 3a and Extended Fig. 4a). Active viral replication, as assessed by sgRNA
153 levels, peaked at 1-2 d.p.i. in nasopharyngeal and tracheal swabs with median values of 4.6 and
154 4.0 log₁₀ copies per ml, respectively (Fig. 3b and Extended Fig. 4b). At 3 d.p.i., viral loads
155 were detected in the BAL with a median value of 4.9 log₁₀ copies per ml of gRNA and 3.2 log₁₀
156 copies per ml of sgRNA, including 3 animals with no detectable sgRNA.

157

158 In comparison, treated animals had a reduction of 2.2 and 3.4 log₁₀ median gRNA VL in
159 tracheal swabs on days 1 and 2 (both $p < 0.01$ to controls), and had undetectable VL after day 4
160 (Fig. 3a and Extended Fig. 4a). The difference was also evident in nasopharyngeal swabs, with
161 treated animals having a reduction of 1.5 and 2.2 log₁₀ gRNA VL on days 1 and 2 (both $p < 0.01$
162 to controls). By day 4, 4/5 treated animals had undetectable gRNA in the nasopharyngeal swabs
163 while one animal (MF7) remained positive with a low residual gRNA signal up to 7 d.p.i..
164 COVA1-18 treatment dramatically hindered viral replication in the upper respiratory tract as
165 evidenced by the absence of detectable sgRNA in the nasopharyngeal and tracheal swabs for
166 all treated animals with the exception of animal (MF9) that showed a low signal at 1 d.p.i. only
167 in the tracheal swabs (Fig. 3b and Extended Fig. 4b). Therefore, in the treated group, most
168 upper respiratory tract gRNA VL likely represents the progressive elimination of the challenge

169 inoculum, and does not result from active replication. The gRNA and sgRNA loads in BAL
170 were also lower in COVA1-18 recipients compared to controls but the difference did not reach
171 statistical significance (Fig. 3a, b, Extended Fig. 4c). Overall, these results demonstrate that a
172 10 mg kg⁻¹ dose of COVA1-18 PrEP dramatically reduced the acquisition and/or early spread
173 of SARS-CoV-2 in the different respiratory compartments.

174

175 Analysis of lung lesions by chest computed tomography (CT) showed that all treated animals
176 had few and small lung lesions as recorded by low CT scores at 3 d.p.i. while 2/5 controls
177 showed mild pulmonary lesions characterized by non-extended ground-glass opacities (GGOs)
178 with scores superior to 5, consistent with what was observed in historic controls (Fig. 3c)²⁵. In
179 addition, we observed that all control animals were lymphopenic at 2 d.p.i., consistent with
180 previous studies^{25,26}, while all treated animals had normal lymphocyte counts throughout the
181 study ($p < 0.01$ for the comparison) (Fig. 3d, Extended Fig. 4d).

182

183 One concern about SARS-CoV-2 vaccines and NAb treatments is the possible generation of
184 suboptimal concentrations of NAb in individuals, which could foster viral escape²⁷. The
185 COVA1-18 treatment resulted in enrichment of subclonal variations in N and ORF1ab, but no
186 treatment-induced escape mutations were detected in the *S* gene when applying standard
187 quality filters (Extended Data Fig. 5).

188

189 **Prediction models refine COVA1-18 dosage**

190 Next, we used a viral dynamic model previously developed in the same SARS-CoV-2 NHP
191 experimental model²⁸ to evaluate the level of protection conferred by COVA1-18. The model
192 considers a target cell limited infection in both nasopharyngeal and tracheal compartments. In
193 addition to the previously developed model, we assumed that sgRNA was a proxy for the total
194 number of non-productively and productively infected cells (see supplementary methods) and
195 we further assumed that COVA1-18 plasma drug concentrations over time, noted $C(t)$, was the
196 driver of drug efficacy. We modeled the changes in $C(t)$ using a standard first order absorption
197 and elimination model, which led estimated half-life of COVA1-18 in plasma of 12.6 days
198 (Extended Data Fig. 6b). We assumed that COVA1-18 reduces infectivity rate in both tracheal
199 and nasopharyngeal compartments with an efficacy, noted $\eta(t)$, determined by the following
200 model $\eta(t) = \frac{C(t)}{C(t) + EC_{50}}$, where EC_{50} is the plasma COVA1-18 concentrations corresponding to
201 a 50% reduction of viral infectivity. The model fitted the viral kinetics well in all animals (Fig.

202 4a, Extended Data Fig. 6a, Extended Data Table 2). In treated animals, EC_{50} was estimated to
203 2.2 and 0.053 $\mu\text{g ml}^{-1}$ in the nasopharynx and trachea, respectively, which is roughly 50 and
204 2000 times lower than the plasma drug concentrations of 109.7 $\mu\text{g ml}^{-1}$ observed on the day of
205 infection (see above). Thus these results confirm that the efficacy of COVA1-18 was very high,
206 with efficacies above 95% and 99.9% in nasopharyngeal and tracheal compartments on the day
207 of infection, respectively (Fig. 4a, Extended Data Fig. 6a). Given the long half-life of the drug,
208 this efficacy could be maintained over time, and we estimated that the mean individual efficacy
209 of the COVA1-18 in the first 10 days following infection ranged between 96.67% and 97.50%
210 in the nasopharynx and between 99.91% and 99.94% in the trachea (Extended Data Table 3).

211

212 Next, we used our model to investigate changes in experimental conditions, such as COVA1-
213 18 dose being administered at a lower dose and/or after the viral challenge (see methods). In
214 all scenarios considered, a dose of 5 mg kg^{-1} was determined to provide nearly similar results
215 than 10 mg kg^{-1} (Fig. 4b, c, Extended Data Fig. 7). A dose of 1 mg kg^{-1} could be sufficient to
216 prevent active viral replication as long as treatment is given prior to infection, but might be
217 insufficient in a therapeutic setting. However, this dose could be relevant if lower doses of
218 virus were used for infection, such as 10^4 or 10^5 PFU (Extended Data Fig. 6c-f).

219

220 Discussion

221 Despite the recent approval of several SARS-CoV-2 vaccines by health authorities, the slow
222 roll-out of vaccination campaigns will not result in resolution of the pandemic in the immediate
223 future. Furthermore, the emergence of viral escape mutants may lead to reduced vaccine
224 efficacy, and some individuals, such as immunocompromised patients or the elderly, may not
225 mount adequate protective immune responses to vaccination. Thus, there is an urgent need to
226 develop effective therapeutics, in particular for individuals with high risk of severe disease.
227 Pre-clinical and clinical studies to evaluate SARS-CoV-2 NAb for prophylaxis and/or
228 treatment and such studies have supported the implementation of several NAb candidates and
229 NAb cocktails for emergency use^{22,29–35}. However, the narrow efficacy range of FDA-approved
230 NAb^{4–6}, together with rapidly spreading new variants complicate treatment strategies^{36–39},
231 highlights the need for additional treatment options, including potent NAb such as COVA1-
232 18.

233 In hACE2-expressing mice and golden Syrian hamsters, COVA1-18 showed remarkable
234 control of SARS-CoV-2 infection. These promising results were confirmed in NHPs, with
235 COVA1-18 given one day prior to infection achieving nearly complete protection in the upper
236 respiratory tract in cynomolgus macaques. Using a viral dynamic model, we estimated that
237 COVA1-18 reduced viral infectivity by >95% and 99.9% in nasopharyngeal and tracheal
238 compartments, respectively. The robustness of these results are reinforced by the high
239 challenge dose that we used, which was 10 to 100-fold higher than in other NHP studies
240 evaluating NABs for PrEP against SARS-CoV-2²⁹⁻³⁴. In fact, the model allowed us to predict,
241 without using additional animals, that protection could be achieved with lower doses of 5 mg
242 kg⁻¹ and 1 mg kg⁻¹ with an inoculum dose of 10⁵ or 10⁴ PFU, both in prophylactic and
243 therapeutic settings (Extended Data Fig. 6, Extended Data Fig. 7).

244

245 How do these levels of efficacy greater than 95% translate into clinical efficacy? In previous
246 work, we estimated that achieving 90% efficacy would be sufficient to confer a high level of
247 protection against infection acquisition if treatment can be administered prophylactically or
248 just after a high-risk contact⁴⁰. In hospitalized patients, where viral load kinetics after admission
249 is associated with the risk of death, we estimated that administration of treatment with an
250 efficacy higher than 90% could reduce the time to viral clearance by more than 3 days in
251 patients over 65 years of age, which could translate into significantly lower rates of mortality
252 in this population⁴¹. Altogether, the results obtained here in a NHP model suggest that COVA1-
253 18 could be a valuable candidate for clinical evaluation.

254

255 A relevant concern is that these results may be jeopardized by the increasing prevalence of
256 mutant strains, which could reduce the sensitivity to NABs. While escape mutations can arise
257 following single NAb treatment as recently demonstrated^{31,42}, COVA1-18 did not select for S
258 protein escape mutants when evaluated as PrEP in NHP. Importantly, studies have determined
259 that COVA1-18 retains high potency against the B.1.1.7 variant, which includes the N501Y
260 mutation^{8,9}. However, as it is derived from IGHV3-66, it will likely lose potency against
261 variants harboring the E484K mutation (*i.e.* the B.1.351 and B.1.1.28 lineages), as recently
262 shown for convalescent plasma and many NABs^{37,38}. This highlights the necessity of using
263 NABs cocktails targeting distinct epitopes. In addition, the half-life of COVA1-18 can be
264 extended by incorporating the LS or YTE⁴³ mutations which can further reduce the protective
265 dose required and reduce the cost of treatment.

266

267 In conclusion, our COVA1-18 *in vitro* data translated into a powerful protective drug in three
268 preclinical models to prevent SARS-CoV-2 replication. Together with our prediction model,
269 these data showed that COVA1-18 could be used in patients at low doses either to prevent
270 infection or to reduce viral loads in a therapeutic setting, with a potential greater impact in
271 high-risk patients. The high *in vivo* efficacy of COVA1-18 and its demonstrated potency
272 against the B.1.1.7. isolate also suggests it is a great candidate for a NAb cocktail.

273 **Main references**

- 274 1. Salama, C. *et al.* Tocilizumab in Patients Hospitalized with Covid-19 Pneumonia. *N. Engl. J.*
275 *Med.* (2020) doi:10.1056/nejmoa2030340.
- 276 2. Horby, P. *et al.* Effect of Dexamethasone in Hospitalized Patients with COVID-19:
277 Preliminary Report. *N. Engl. J. Med.* (2020) doi:10.1101/2020.06.22.20137273.
- 278 3. Update to living WHO guideline on drugs for covid-19. *BMJ* (2020) doi:10.1136/bmj.m4475.
- 279 4. Weinreich, D. M. *et al.* REGN-COV2, a Neutralizing Antibody Cocktail, in Outpatients with
280 Covid-19. *N. Engl. J. Med.* **384**, (2021).
- 281 5. Chen, P. *et al.* SARS-CoV-2 Neutralizing Antibody LY-CoV555 in Outpatients with Covid-
282 19. *N. Engl. J. Med.* **384**, (2021).
- 283 6. A Neutralizing Monoclonal Antibody for Hospitalized Patients with Covid-19. *N. Engl. J.*
284 *Med.* NEJMoa2033130 (2020) doi:10.1056/NEJMoa2033130.
- 285 7. Brouwer, P. J. M. *et al.* Potent neutralizing antibodies from COVID-19 patients define
286 multiple targets of vulnerability. *Science* **369**, (2020).
- 287 8. Rees-Spear, C. *et al.* The impact of Spike mutations on SARS-CoV-2 neutralization. Preprint
288 at 10.1101/2021.01.15.426849.
- 289 9. Shen, X. *et al.* SARS-CoV-2 variant B.1.1.7 is susceptible to neutralizing antibodies elicited
290 by ancestral Spike vaccines. Preprint at 10.1101/2021.01.27.428516.
- 291 10. COVID-19 Dashboard by the Center for Systems Science and Engineering (CSSE) at Johns
292 Hopkins University (JHU). <https://coronavirus.jhu.edu/map.html> (2021).
- 293 11. Zost, S. J. *et al.* Rapid isolation and profiling of a diverse panel of human monoclonal
294 antibodies targeting the SARS-CoV-2 spike protein. *Nat. Med.* **26**, (2020).
- 295 12. Cao, Y. *et al.* Potent Neutralizing Antibodies against SARS-CoV-2 Identified by High-
296 Throughput Single-Cell Sequencing of Convalescent Patients' B Cells. *Cell* **182**, (2020).
- 297 13. Hansen, J. *et al.* Studies in humanized mice and convalescent humans yield a SARS-CoV-2
298 antibody cocktail. *Science* **369**, (2020).
- 299 14. Wu, Y. *et al.* A noncompeting pair of human neutralizing antibodies block COVID-19 virus
300 binding to its receptor ACE2. *Science* **368**, (2020).
- 301 15. Schmidt, F. *et al.* Measuring SARS-CoV-2 neutralizing antibody activity using pseudotyped
302 and chimeric viruses. *J. Exp. Med.* **217**, (2020).
- 303 16. Almahboub, S. A., Algaissi, A., Alfaleh, M. A., ElAssouli, M.-Z. & Hashem, A. M.
304 Evaluation of Neutralizing Antibodies Against Highly Pathogenic Coronaviruses: A Detailed
305 Protocol for a Rapid Evaluation of Neutralizing Antibodies Using Vesicular Stomatitis Virus
306 Pseudovirus-Based Assay. *Front. Microbiol.* **11**, (2020).
- 307 17. Korber, B. *et al.* Tracking Changes in SARS-CoV-2 Spike: Evidence that D614G Increases
308 Infectivity of the COVID-19 Virus. *Cell* **182**, (2020).

- 309 18. Yurkovetskiy, L. *et al.* Structural and Functional Analysis of the D614G SARS-CoV-2 Spike
310 Protein Variant. *Cell* **183**, (2020).
- 311 19. Plante, J. A. *et al.* Spike mutation D614G alters SARS-CoV-2 fitness. *Nature* (2020)
312 doi:10.1038/s41586-020-2895-3.
- 313 20. Mansbach, R., Chakraborty, S., Nguyen, K., Montefiori, D. & Korber, B. The SARS-CoV-2
314 Spike Variant D614G Favors an Open Conformational State. Preprint at
315 10.1101/2020.07.26.219741.
- 316 21. Volz, E. *et al.* Evaluating the Effects of SARS-CoV-2 Spike Mutation D614G on
317 Transmissibility and Pathogenicity. *Cell* (2020) doi:10.1016/j.cell.2020.11.020.
- 318 22. Hassan, A. O. *et al.* A SARS-CoV-2 Infection Model in Mice Demonstrates Protection by
319 Neutralizing Antibodies. *Cell* **182**, (2020).
- 320 23. Rathnasinghe, R. *et al.* Comparison of transgenic and adenovirus hACE2 mouse models for
321 SARS-CoV-2 infection. *Emerg. Microbes Infect.* **9**, 2433–2445 (2020).
- 322 24. Muñoz-Fontela, C. *et al.* Animal models for COVID-19. *Nature* vol. 586 509–515 (2020).
- 323 25. Maisonnasse, P. *et al.* Hydroxychloroquine use against SARS-CoV-2 infection in non-human
324 primates. *Nature* **585**, 584–587 (2020).
- 325 26. Brouwer, P. J. M. *et al.* Two-component spike nanoparticle vaccine protects macaques from
326 SARS-CoV-2 infection. *Cell* 2020.11.07.365726 (2021) doi:10.1016/j.cell.2021.01.035.
- 327 27. Andreano, E. *et al.* SARS-CoV-2 escape &in vitro& from a highly
328 neutralizing COVID-19 convalescent plasma. Preprint at doi:10.1101/2020.12.28.424451.
- 329 28. Gonçalves, A. *et al.* Viral dynamic modeling of SARS-CoV-2 in non-human primates. *Res. Sq.*
330 (2021) doi:10.21203/rs.3.rs-50301/v1.
- 331 29. Baum, A. *et al.* REGN-COV2 antibodies prevent and treat SARS-CoV-2 infection in rhesus
332 macaques and hamsters. *Science* (2020) doi:10.1126/science.abe2402.
- 333 30. Zost, S. J. *et al.* Potently neutralizing and protective human antibodies against SARS-CoV-2.
334 *Nature* **584**, (2020).
- 335 31. Jones, B. E. *et al.* Title: LY-CoV555, a rapidly isolated potent neutralizing antibody, provides
336 protection in a non-human primate model of SARS-CoV-2 infection.
337 doi:10.1101/2020.09.30.318972.
- 338 32. Shi, R. *et al.* A human neutralizing antibody targets the receptor-binding site of SARS-CoV-2.
339 *Nature* **584**, (2020).
- 340 33. Wang, S. *et al.* Characterization of neutralizing antibody with prophylactic and therapeutic
341 efficacy against SARS-CoV-2 in rhesus monkeys. *Nat. Commun.* **11**, (2020).
- 342 34. Li, D. *et al.* The functions of SARS-CoV-2 neutralizing and infection-enhancing antibodies in
343 vitro and in mice and nonhuman primates. Preprint at 10.1101/2020.12.31.424729.
- 344 35. Fagre, A. C. *et al.* A Potent SARS-CoV-2 Neutralizing Human Monoclonal Antibody That
345 Reduces Viral Burden and Disease Severity in Syrian Hamsters. *Front. Immunol.* **11**, (2020).

- 346 36. Wu, K. *et al.* mRNA-1273 vaccine induces neutralizing antibodies against spike mutants from
347 global SARS-CoV-2 variants. Preprint at 10.1101/2021.01.25.427948.
- 348 37. Wang, P. *et al.* Increased Resistance of SARS-CoV-2 Variants B.1.351 and B.1.1.7 to
349 Antibody Neutralization. Preprint at 10.1101/2021.01.25.428137.
- 350 38. Starr, T. N. *et al.* Prospective mapping of viral mutations that escape antibodies used to treat
351 COVID-19. *Science* (2021) doi:10.1126/science.abf9302.
- 352 39. Wibmer, C. K. *et al.* SARS-CoV-2 501Y.V2 escapes neutralization by South African COVID-
353 19 donor plasma. Preprint at 10.1101/2021.01.18.427166.
- 354 40. Czuppon, P. *et al.* Success of prophylactic antiviral therapy for SARS-CoV-2: predicted
355 critical efficacies and impact of different drug-specific mechanisms of action. Preprint at
356 10.1101/2020.05.07.20092965.
- 357 41. Néant, N. *et al.* Modeling SARS-CoV-2 viral kinetics and association with mortality in
358 hospitalized patients: results from the French Covid-19 cohort. *Proc Natl Acad Sci U S A*
359 (2021).
- 360 42. Baum, A. *et al.* Antibody cocktail to SARS-CoV-2 spike protein prevents rapid mutational
361 escape seen with individual antibodies. *Science* **369**, (2020).
- 362 43. Saunders, K. O. Conceptual Approaches to Modulating Antibody Effector Functions and
363 Circulation Half-Life. *Front. Immunol.* **10**, (2019).

364

365 **Methods**

366 **IgG, Fab and soluble viral protein expression**

367 COVA1-18 was isolated from a participant in the “COVID-19 Specific Antibodies” (COSCA)
368 study as described⁷. The COSCA study was conducted at the Amsterdam University Medical
369 Centre, location AMC, the Netherlands and approved by the local ethical committee of the
370 AMC (NL 73281.018.20). COVA1-18 IgG was produced in HEK293F suspension cells as
371 previously described⁷. COVA1-18 His-tagged Fab was produced in ExpiCHO cells as
372 previously described⁴⁴. Spike and RBD proteins were produced and purified as previously
373 described⁷.

374

375 **Bio-layer interferometry**

376 The affinity of COVA1-18 IgG and His-tagged Fab versions were determined using Ni-NTA
377 biosensors (ForteBio) onto which 20 $\mu\text{g ml}^{-1}$ of SARS-CoV-2 RBD in running buffer (PBS,
378 0.02% Tween-20, 0.1% BSA) was loaded for 300 s as previously described⁴⁴. The association
379 rate and dissociation step were assessed over a 120 s step each. Serially diluted IgG (50, 100,
380 200 and 400 nM) and Fab (100, 200, 400 and 800 nM) were tested and an anti-HIV-1 His-
381 tagged Fab at 800 nM in running buffer was included as negative control. K_{DS} were determined
382 using ForteBio Octet CFR software using a 1:2 fitting model for IgGs and a 1:1 fitting model
383 for Fabs. The apparent affinity of COVA1-18 IgG to the SARS-CoV-2 S trimer was determined
384 as described above except that 20 $\mu\text{g ml}^{-1}$ SARS-CoV-2 S 2P Fld His protein was loaded
385 instead of RBD. The COVA1-18 IgG avidity effect was further evaluated by titrating the loaded
386 SARS-CoV-2 RBD (5, 1, 0.2 and 0.04 $\mu\text{g ml}^{-1}$). An additional loading step using His-tagged
387 HIV-1 gp41 was performed to minimize background binding of His-tagged Fabs to the
388 biosensor and both the COVA1-18 IgG and Fab concentrations were set at 250 nM. All other
389 steps were performed as described above.

390

391 **Ni-NTA-capture ELISA**

392 SARS-CoV-2, SARS-CoV, MERS, HKU1, 229E and NL63 S His-tagged proteins were loaded
393 at 2 $\mu\text{g ml}^{-1}$ in TBS/2% skimmed milk (100 $\mu\text{l/well}$) on 96-well Ni-NTA plates (Qiagen) for 2
394 h at room temperature (RT). Three-fold serially diluted COVA NAb were then added onto the
395 plates for 2 h at RT followed by the addition goat anti-human IgG-HRP (Jackson
396 Immunoresearch) secondary Ab (1:3000) for 1 h at RT. The plates were developed for 3 min

397 using TMB solution then stopped, optical densities measured at 450 nm on a spectrophotometer
398 and data graphed using GraphPad Prism software (v8.3.0).

399

400 **Detection of human IgG in NHP fluid**

401 Detection of COVA1-18 in NHP samples determined by ELISA using a protocol adapted from
402 others³⁰. Briefly, half area high binding 96-well plates (Greiner Bio-One) were coated
403 overnight with goat anti-Human IgG H+L (monkey pre-adsorbed) at 1 $\mu\text{g ml}^{-1}$ in PBS. The
404 plates were then blocked in casein buffer (Thermo Scientific) for 2 h at RT. Serum and mucosal
405 samples were serially diluted and loaded onto the plates as well as serially diluted COVA1-18
406 as the standard. Following a 1 h RT incubation, goat anti-Human IgG (monkey adsorbed)-HRP
407 secondary antibody (Southern Biotech) was added for serum samples (1:4000). For mucosal
408 samples, goat anti-Human IgG (monkey adsorbed)-BIOT (Southern Biotech) was added at
409 1:10000 dilution. After 1 h RT incubation, serum sample plates were ready for development.
410 For mucosal samples, an additional 1 h incubation with poly-HRP40 (Fitzgerald) (1:10000)
411 was necessary. The plates were then developed for 5 min, the optical densities measured at 450
412 nm on a spectrophotometer and raw data exported and analyzed using Microsoft Excel and
413 GraphPad Prism (v8.3.0) software. The COVA1-18 concentration in a specific sample was
414 determined by interpolating OD values from dilutions that fell into the linear range of the
415 standard curve of the matching ELISA plate.

416

417 **Cynomolgus monkey IgG ELISA**

418 Half area high binding 96-well plates were coated overnight (4 °C) with goat anti-Human IgG
419 λ and goat anti-Human IgG κ (Southern Biotech), 1:2000 (each) in PBS, 50 $\mu\text{l/well}$. The plates
420 were washed (1X TBS – 0,05% Tween20) and block for 2 h at RT with 50 $\mu\text{l/well}$ casein buffer.
421 Serially diluted mucosal and serum samples were loaded onto the plates. Serially diluted
422 polyclonal cynomolgus IgG (Molecular Innovations) was used as standard. Following a 1 h
423 incubation at RT, mouse anti-Monkey IgG Fc-BIOT (Southern Biotech) was loaded onto the
424 plate (1:50000). After 1 h at RT, poly-HRP40 was added (1:10000) and the plates incubated
425 for 1 h. Finally, the plates were washed 5 times, developed for 5 min, and analysed as described
426 above.

427

428 **Pseudovirus neutralization assay**

429 Neutralization assays were performed using SARS-CoV-2 S-pseudotyped HIV-1 virus and
430 HEK293T hACE2 cells as described previously¹⁵. In brief, pseudotyped virus was produced

431 by co-transfecting expression plasmids of SARS-CoV-2 Δ 19 S proteins (GenBank MT449663.1)
432 with an HIV backbone expressing NanoLuc luciferase (pHIV-1_{NL4-3} Δ Env-NanoLuc) in
433 HEK293T cells (ATCC, CRL-11268). After 2 days, the cell culture supernatants containing
434 SARS-CoV-2 S-pseudotyped HIV-1 viruses were harvested and stored at -80 °C. HEK293T
435 hACE2 cells were seeded 20,000 cells/well in a flat-bottom 96-well plates one day prior to the
436 start of the neutralization assay. COVA1-18 IgG and His₆-tagged Fab as well as heat-
437 inactivated serum samples were serially diluted in 3-fold steps using cell culture medium and
438 then mixed with pseudotyped virus in a 1:1 ratio and incubated for 1 h at 37 °C. The mixtures
439 were then added to the HEK293T hACE2 cells in a 1:1 medium to mixture ratio. The final
440 starting concentration for IgGs was 20 μ g ml⁻¹ and 13.33 μ g ml⁻¹ for Fab. The cells were then
441 incubated at 37 °C for 48 h followed by one PBS wash and lysis buffer addition. The luciferase
442 activity in the cell lysates was measured using the Nano-Glo Luciferase Assay System
443 (Promega) and GloMax Discover microplate reader. Relative luminescence units (RLU) were
444 normalized to those from positive control wells where cells were infected with SARS-CoV-2
445 pseudovirus without IgG, Fab or serum. The inhibitory concentration (IC₅₀) and neutralization
446 titers (ID₅₀) were determined as the IgG/Fab concentration or serum dilution at which
447 infectivity was inhibited by 50%.

448
449 Pseudotyped Vesicular Stomatitis Virus (VSV Δ G) particles displaying SARS-CoV-2 Δ 19 S and
450 containing a luciferase reporter were used as previously described¹⁶. Two-fold dilution series
451 of COVA1-18 were prepared in complete medium, pseudotyped virus added and the mixture
452 incubated for 1 h at 37 °C. The virus-antibody mixtures were then loaded onto plates seeded
453 with Vero E6 cells 24 h prior this step. Following a 20 h incubation 37 °C, the luciferase
454 substrate was added to lysed cells and RLU determined and analyzed as described above.

455

456 **Ethics and biosafety statement**

457 Female golden Syrian hamsters, aged 6-7 weeks, were housed in the ABSL-4 facility of the
458 Galveston National Laboratory. The animal protocol # 2004049 was approved by the
459 Institutional Animal Care and Use Committee (IACUC) of the University of Texas Medical
460 Branch at Galveston (UTMB).

461

462 The mouse experimental study was approved by the Icahn School of Medicine at Mount Sinai
463 Institutional Animal Care and Use Committee (IACUC-2017-0170 and IACUC-2017-0330).

464

465 Male and female cynomolgus macaques (*Macaca fascicularis*), aged 3-6 years and originating
466 from Mauritian AAALAC certified breeding centers were used in this study. All animals were
467 housed in IDMIT infrastructure facilities (CEA, Fontenay-aux-roses), under BSL-2 and BSL-
468 3 containment when necessary (Animal facility authorization #D92-032-02, Préfecture des
469 Hauts de Seine, France) and in compliance with European Directive 2010/63/EU, the French
470 regulations and the Standards for Human Care and Use of Laboratory Animals, of the Office
471 for Laboratory Animal Welfare (OLAW, assurance number #A5826-01, US). The protocols
472 were approved by the institutional ethical committee “Comité d’Ethique en Expérimentation
473 Animale du Commissariat à l’Energie Atomique et aux Energies Alternatives” (CEtEA #44)
474 under statement number A20-011. The study was authorized by the “Research, Innovation and
475 Education Ministry” under registration number APAFIS#24434-2020030216532863.

476

477 **Ethics committee**

478 All information on the ethics committee is available at [https://cache.media.enseignementsup-
479 recherche.gouv.fr/file/utilisation_des_animaux_fins_scientifiques/22/1/comiteethiqueea17_ju
480 in2013_257221.pdf](https://cache.media.enseignementsup-recherche.gouv.fr/file/utilisation_des_animaux_fins_scientifiques/22/1/comiteethiqueea17_ju_in2013_257221.pdf)

481

482 **Viruses and cells**

483 For the macaques studies, SARS-CoV-2 virus (hCoV-19/France/ IDF0372/2020 strain) was
484 isolated by the National Reference Center for Respiratory Viruses (Institut Pasteur, Paris,
485 France) as previously described⁴⁵ and produced by two passages on Vero E6 cells in DMEM
486 (Dulbecco’s Modified Eagles Medium) without FBS, supplemented with 1% P/S (penicillin at
487 10,000 U ml⁻¹ and streptomycin at 10,000 µg ml⁻¹) and 1 µg ml⁻¹ TPCK-trypsin at 37 °C in a
488 humidified CO₂ incubator and titrated on Vero E6 cells. Whole genome sequencing was
489 performed as described⁴⁵ with no modifications observed compared with the initial specimen
490 and sequences were deposited after assembly on the GISAID EpiCoV platform under accession
491 number ID EPI_ISL_406596. Sequencing analysis revealed two clonal mutations, one in the *S*
492 gene (22661G>T : V367F, non-synonymous) and one in the *ORF3a* gene (26144G>T : G251V,
493 non-synonymous), which were already present in the challenge inoculum.

494

495 **Animals and study design**

496 Seven week old female Balb/cJ mice (Jackson Laboratories Bar Harbor, ME) were anesthetized
497 before being administered with 2.5 x 10⁸ PFU of human adenovirus type 5 encoding the human
498 angiotensin converting enzyme-2 receptor (Ad5-hACE2) 5-days prior to challenge with SARS-

499 CoV-2, as previously described^{22,23}. Animals were transferred to the BSL-3 facility where two
500 groups of n = 5 mice per group received 10 mg kg⁻¹ of COVA1-18 intraperitoneally 24 h prior
501 to, or post-infection with 10⁴ PFU SARS-CoV-2 in 50 µl PBS. A control group of n = 3 mice
502 received 50 µl PBS. Mice were euthanized 3 d.p.i. and lungs harvested to quantify viral lung
503 titers. Lungs were homogenized in PBS using a Beadblaster Microtube homogenizer
504 (Benchmark Scientific). SARS-CoV-2 plaque assay was performed on 10-fold serial dilutions
505 of lung homogenates prepared in 0.2% bovine serum albumin (BSA) in PBS that were plated
506 onto a Vero E6 cells monolayer and incubated with shaking for 1 h. Inoculum was removed
507 and plates were overlaid with Minimal Essential Media (MEM) containing 2% FBS/0.05%
508 oxoid agar and incubated for 72 h at 37°C. Plates were fixed with 4% formaldehyde overnight,
509 stained with a mAb cocktail composed of SARS-CoV-2 spike and SARS-CoV-2 nucleoprotein
510 (Center for Therapeutic Antibody Discovery; NP1C7C7) followed by anti-Mouse IgG-HRP
511 (Abcam ab6823) and developed using KPL TrueBlue peroxidase substrate (Seracare; 5510-
512 0030).

513

514 Golden Syrian hamsters were randomly assigned to two groups of n = 5 and microchipped 24
515 h before SARS-CoV-2 challenge. On the day of challenge, hamsters were anesthetized with
516 ketamine/xylazine and challenged by the intranasal route with 10⁵ PFU of SARS-CoV-2
517 diluted in sterile PBS in the total volume 100 µl. Body weight and body temperature were
518 measured each day, starting at day 0. Twenty four hours post-challenge, hamsters were treated
519 with 10 mg kg⁻¹ of COVA1-18 diluted in 0.5 ml of sterile PBS via the intraperitoneal route.
520 The control group of animals received an equal volume of sterile PBS via the intraperitoneal
521 route. All animals were euthanized 72 h post-infection with an overdose of anesthetic
522 (isoflurane or ketamine/xylazine) followed by bilateral thoracotomy, and terminal blood and
523 lungs were collected at necropsy. Right lungs were frozen in 5 ml L-15 Leibowitz medium
524 (Gibco) with 10% FBS. Tissue sections were homogenized in bead beater tubes, weighed, and
525 supernatants were titrated per standard protocol. Briefly, of 10-fold dilutions of supernatants at
526 100 µl per well were placed atop of Vero-E6 monolayers in 96-well plates, the plates were
527 incubated for 1 h, supernatants were replaced by methyl cellulose overlay, incubated for 3 days
528 at 5% CO₂ and 37 °C. The plates were fixed with formalin, removed from BSL-4 according the
529 approved protocol, and plaques counted to determine the viral titers.

530

531 Ten female cynomolgus macaques were randomly assigned between the control and treated
532 groups to evaluate the efficacy of COVA1-18 prophylaxis. The treated group (n = 5) received

533 one bolus dose of COVA-18 human IgG1 monoclonal antibody (10 mg kg⁻¹) by the intravenous
534 route in the saphenous vein one day prior to challenge, while control animals (n = 5) received
535 no treatment. All animals were then exposed to a total dose of 10⁶ PFU of SARS-CoV-2
536 (BetaCoV/France/IDF/0372/2020; passaged twice in VeroE6 cells) *via* the combination of
537 intranasal and intratracheal routes (day 0), using atropine (0.04 mg kg⁻¹) for pre-medication
538 and ketamine (5 mg kg⁻¹) with medetomidine (0.05 mg kg⁻¹) for anesthesia. Animals were
539 observed daily and clinical exams were performed at baseline, daily for one week, and then
540 twice weekly, on anaesthetized animals using ketamine (5 mg kg⁻¹) and medetomidine (0.05
541 mg kg⁻¹). Body weight and rectal temperature were recorded and blood, as well as
542 nasopharyngeal, tracheal and rectal swabs, were collected. Broncho-alveolar lavages (BAL)
543 were performed using 50 ml sterile saline on 3 d.p.i. Chest CT was performed at 3 d.p.i. in
544 anesthetized animals using tiletamine (4 mg kg⁻¹) and zolazepam (4 mg kg⁻¹). Blood cell counts,
545 haemoglobin and haematocrit were determined from EDTA blood using a DHX800 analyzer
546 (Beckman Coulter).

547

548 One male and one female cynomolgus macaques received the treatment as described above for
549 the pharmacokinetic and pharmacodynamics (PK/PD) study. Blood was sampled before and 2,
550 4, 6 and 24 h post-treatment. Saliva, nasopharyngeal and tracheal fluids were sampled before
551 and 24 h post-treatment. Twenty-four hours post-treatment, animals were euthanized and their
552 lungs, heart, kidney, liver, spleen, trachea and brain were sampled, rinsed with PBS and around
553 100 mg of tissue was homogenized in 500 µl of PBS with a Precellys and stored at -80°C.

554

555 **Virus quantification in NHP samples**

556 Upper respiratory (nasopharyngeal and tracheal) and rectal specimens were collected with
557 swabs (Viral Transport Medium, CDC, DSR-052-01). Tracheal swabs were performed by
558 insertion of the swab above the tip of the epiglottis into the upper trachea at approximately 1.5
559 cm of the epiglottis. All specimens were stored between 2°C and 8°C until analysis by RT-
560 qPCR with a plasmid standard concentration range containing an RdRp gene fragment
561 including the RdRp-IP4 RT-PCR target sequence. SARS-CoV-2 E gene subgenomic mRNA
562 (sgRNA) levels were assessed by RT-qPCR using primers and probes previously described^{46,47}:
563 leader-specific primer sgLeadSARSCoV2-F CGATCTCTTG TAGATCTGTTCTC, E-
564 Sarbeco-R primer ATATTGCAGCAGTACGCACACA and E-Sarbeco probe HEX-
565 AACTAGCCATCCTTACTGCGCTTCG-BHQ1. The protocol describing the procedure for
566 the detection of SARS-CoV-2 is available on the WHO website

567 ([https://www.who.int/docs/default-source/coronaviruse/real-time-rt-pcr-assays-for-the-](https://www.who.int/docs/default-source/coronaviruse/real-time-rt-pcr-assays-for-the-detection-of-sars-cov-2-institut-pasteur-paris.pdf?sfvrsn=3662fcb6_2)
568 [detection-of-sars-cov-2-institut-pasteur-paris.pdf?sfvrsn=3662fcb6_2](https://www.who.int/docs/default-source/coronaviruse/real-time-rt-pcr-assays-for-the-detection-of-sars-cov-2-institut-pasteur-paris.pdf?sfvrsn=3662fcb6_2)).

569

570 **Chest CT and image analysis**

571 Lung images were acquired using a computed tomography (CT) system (Vereos-Ingenuity,
572 Philips) as previously described^{25,26}. Lesions were defined as ground glass opacity, crazy-
573 paving pattern, consolidation or pleural thickening as previously described^{32,48}. Lesions and
574 scoring were assessed in each lung lobe blindly and independently by two persons and the final
575 results were established by consensus. Overall CT scores include the lesion type (scored from
576 0 to 3) and lesion volume (scored from 0 to 4) summed for each lobe as previously
577 described^{25,26}.

578

579 **Viral sequencing**

580 10 RNA samples from nasopharyngeal swabs at day 3 post-exposure were selected for
581 sequencing along with the inoculum. cDNA and multiplex PCR reactions were prepared
582 following the ARTIC SARS-CoV-2 sequencing protocol v2⁴⁹. V3 primer scheme
583 (<https://github.com/artic-network/primer-schemes/tree/master/nCoV-2019/V3>) was used to
584 perform the multiplex PCR for SARS-CoV-2. All samples were run for 35 cycles in the two
585 multiplex PCRs. Pooled and cleaned PCR reactions were quantified using QubitTM
586 fluorometer (Invitrogen). The Ligation Sequencing kit (SQK-LSK109; Oxford Nanopore
587 Technologies) was used to prepare the library following the manufacturer's protocol ("PCR
588 tiling of COVID-19 virus", release F; Oxford Nanopore Technologies). Twenty-four samples
589 were multiplexed using Native Barcoding Expansion 1-12 and Native Barcoding Expansion
590 13-24 kits (EXP-NBD104 and EXP-NBD114; Oxford Nanopore Technologies). Two libraries
591 of 24 samples were prepared independently and quantified by QubitTM fluorometer
592 (Invitrogen). After the quality control, two R9.4 flowcells (FLO-MIN106; Oxford Nanopore
593 Technologies) were primed as described in the manufacturer's protocol and loaded with 45 and
594 32 ng of library. Sequencing was performed on a GridION (Oxford Nanopore Technologies)
595 for 72h with high-accuracy Guppy basecalling (v3.2.10). After sequencing, demultiplexing was
596 performed using Guppy v4.0.14 with the option `--require_barcodes_both_ends` to ensure high
597 quality demultiplexing. Reads were then filtered by Nanoplot v1.28.1 based on length and
598 quality to select high quality reads. Then, reads were aligned on the SARS-CoV-2 reference
599 genome NC_045512.2 using minimap2 v2.17. Primary alignments were filtered based on reads
600 length alignment and reads identity. Reads were basecalled and demultiplexed with Guppy

601 4.0.14. The potential clonal and subclonal variants were detected with a custom pipeline based
602 on ARTIC network workflow. Longshot v0.4.1 was used for variant detection. The potential
603 subclonal variants were manually curated by comparing the generated VCF files and visual
604 inspection of the alignments in IGV browser.

605

606 **Statistical analysis**

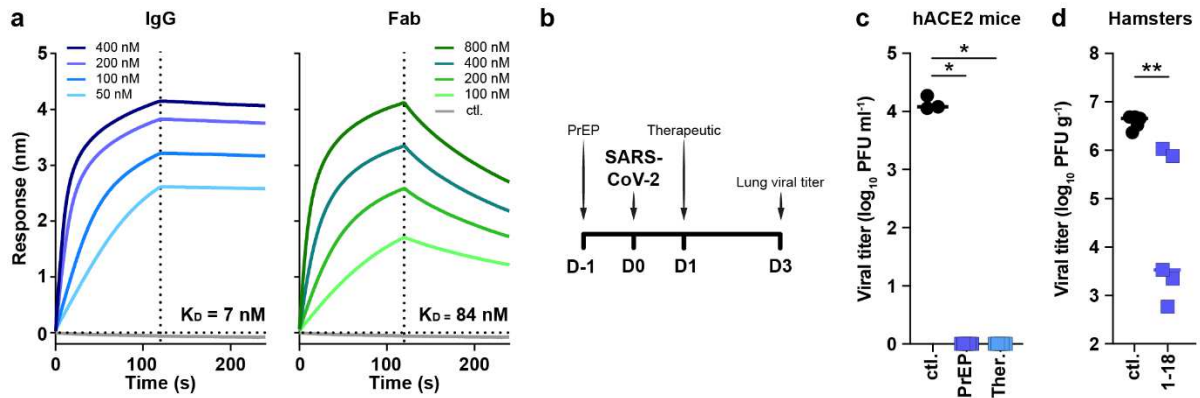
607 Statistical analysis of Syrian hamsters and hACE2 mice lung viral titers as well as for NHP
608 gRNA and sgRNA were carried out using Mann-Whitney unpaired t-test in GraphPad Prism
609 software (v8.3.0).

610 **Methods references**

- 611 44. Liu, H. *et al.* Cross-Neutralization of a SARS-CoV-2 Antibody to a Functionally Conserved
612 Site Is Mediated by Avidity. *Immunity* **53**, 1272–1280.e5 (2020).
- 613 45. Lescure, F. X. *et al.* Clinical and virological data of the first cases of COVID-19 in Europe: a
614 case series. *Lancet Infect. Dis.* **20**, 697–706 (2020).
- 615 46. Corman, V. M. *et al.* Detection of 2019 novel coronavirus (2019-nCoV) by real-time RT-PCR.
616 *Eurosurveillance* **25**, (2020).
- 617 47. Wölfel, R. *et al.* Virological assessment of hospitalized patients with COVID-2019. *Nature*
618 **581**, 465–469 (2020).
- 619 48. Pan, F. *et al.* Time course of lung changes at chest CT during recovery from Coronavirus
620 disease 2019 (COVID-19). *Radiology* **295**, 715–721 (2020).
- 621 49. Tyson, J. R. *et al.* Improvements to the ARTIC multiplex PCR method for SARS-CoV-2
622 genome sequencing using nanopore. Preprint at 10.1101/2020.09.04.283077.
- 623 50. Coughlan, L. *et al.* In Vivo Retargeting of Adenovirus Type 5 to $\alpha\beta 6$ Integrin Results in
624 Reduced Hepatotoxicity and Improved Tumor Uptake following Systemic Delivery. *J. Virol.*
625 **83**, 6416–6428 (2009).
- 626 51. Coughlan, L. *et al.* Ad5:Ad48 Hexon Hypervariable Region Substitutions Lead to Toxicity and
627 Increased Inflammatory Responses Following Intravenous Delivery. *Mol. Ther.* **20**, 2268–
628 2281 (2012).
- 629 52. Baccam, P., Beauchemin, C., Macken, C. A., Hayden, F. G. & Perelson, A. S. Kinetics of
630 Influenza A Virus Infection in Humans. *J. Virol.* **80**, 7590–7599 (2006).
- 631 53. Best, K. *et al.* Zika plasma viral dynamics in nonhuman primates provides insights into early
632 infection and antiviral strategies. *Proc. Natl. Acad. Sci. U. S. A.* **114**, 8847–8852 (2017).
- 633 54. Pawelek, K. A. *et al.* Modeling within-host dynamics of influenza virus infection including
634 immune responses. *PLoS Comput. Biol.* **8**, (2012).
- 635 55. Dubois, A., Bertrand, J. & Mentré, F. Mathematical Expressions of the Pharmacokinetic and
636 Pharmacodynamic Models implemented in the PFIM software. *PFIM Gr.* (2011).
- 637 56. Comets, E., Lavenu, A. & Lavielle, M. Parameter estimation in nonlinear mixed effect models
638 using saemix, an R implementation of the SAEM algorithm. *J. Stat. Softw.* **80**, (2017).
- 639 57. Delyon, B., Lavielle, M. & Moulines, E. Convergence of a stochastic approximation version of
640 the EM algorithm. *Ann. Stat.* **27**, (1999).

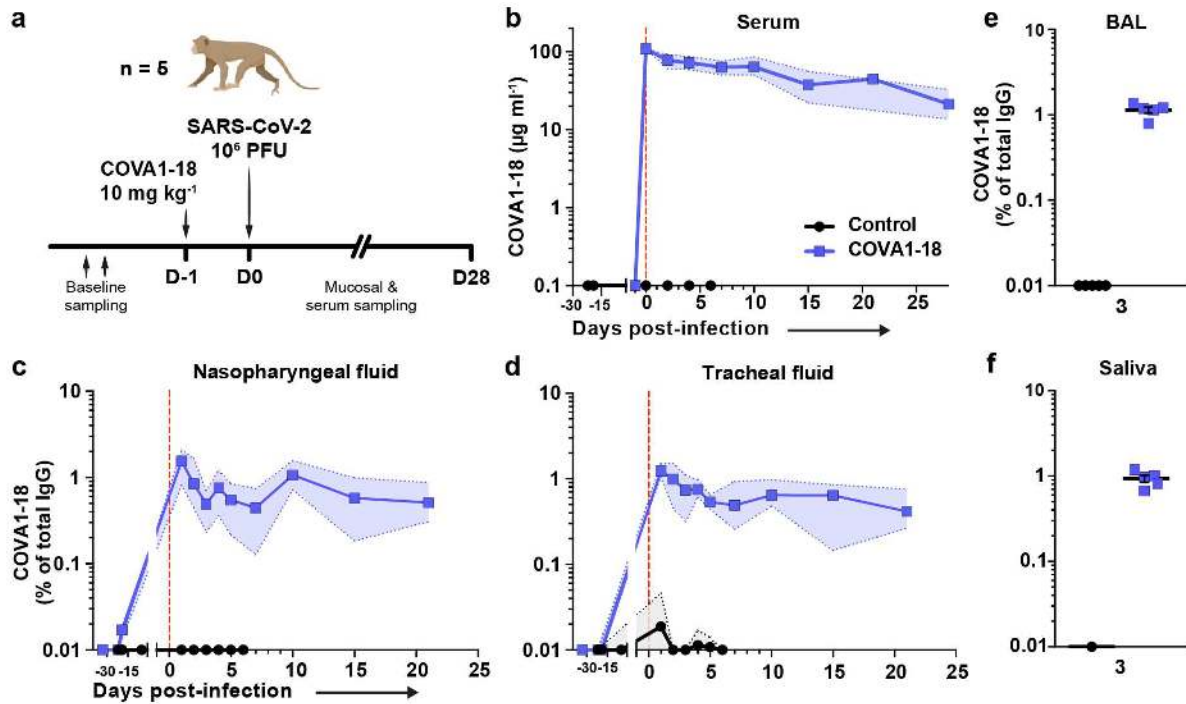
641

642



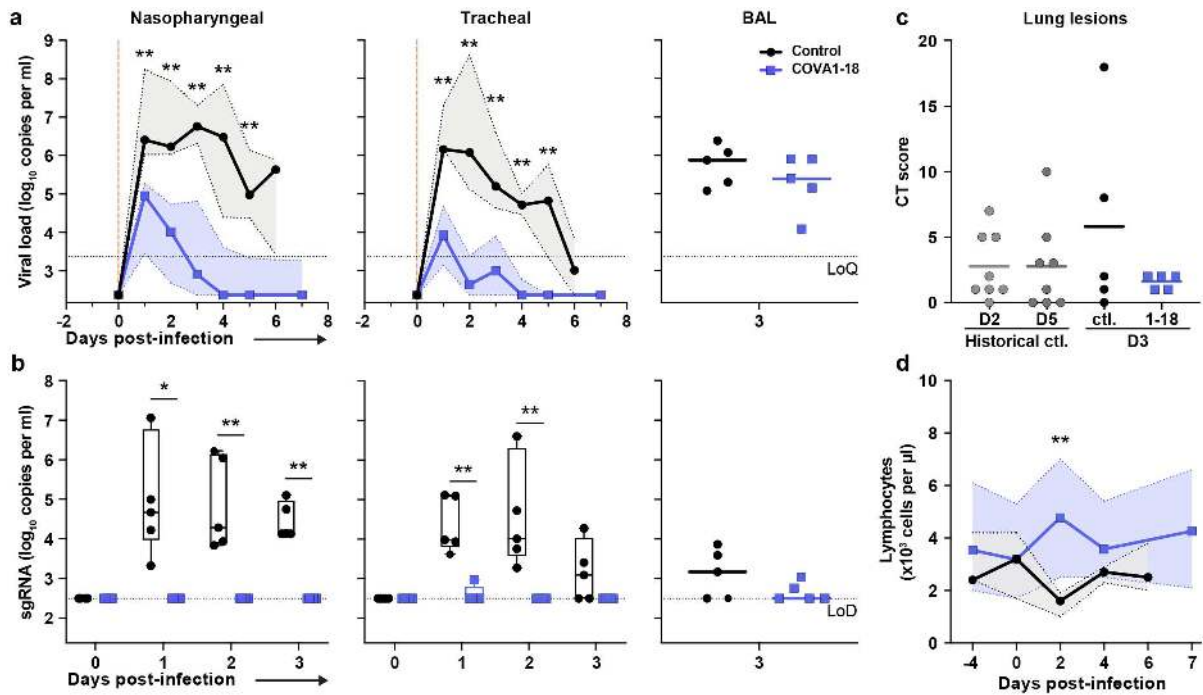
643
644
645
646
647
648
649
650
651

Figure 1. COVA1-18 avidity and SARS-CoV-2 protection in rodents. (a) Bi-layer interferometry sensorgrams comparing COVA1-18 IgG and Fab binding to RBD. K_D s are indicated. Representative of 3 independent experiments. (b) Study design with $n = 5$ per group, except mouse control group ($n = 3$). Hamsters were infected with 10^5 PFU on day 0 and treated on day 1. Mice received COVA1-18 24 h prior to or after exposure to 10^4 PFU. Lung viral titers at 3 d.p.i. are shown for mice (c) and hamsters (d). Bars indicate medians. Mann-Whitney unpaired t-test, p values: $* < 0.05$, $** < 0.01$. Ctl., control group; PrEP, pre-exposure prophylaxis; Ther., therapeutic.



652
653
654
655
656
657
658
659

Figure 2. COVA1-18 serum and mucosal pharmacokinetic in infected cynomolgus macaques. (a) Study design. Two groups of $n = 5$ were exposed to 10^6 PFU of SARS-CoV-2 (intranasal and intratracheal routes). Treated animals received 10 mg kg^{-1} of COVA1-18 1 day before challenge. (b) COVA1-18 serum concentration (mean with range). COVA1-18 concentration reported as percent of total cynomolgus IgG in heat-inactivated (c) nasopharyngeal fluid, (d) tracheal fluid (means with range), (e) bronchoalveolar lavage (BAL) and (f) saliva (means \pm SEMs). The red dashed line indicates challenge day.



661

662

663

664

665

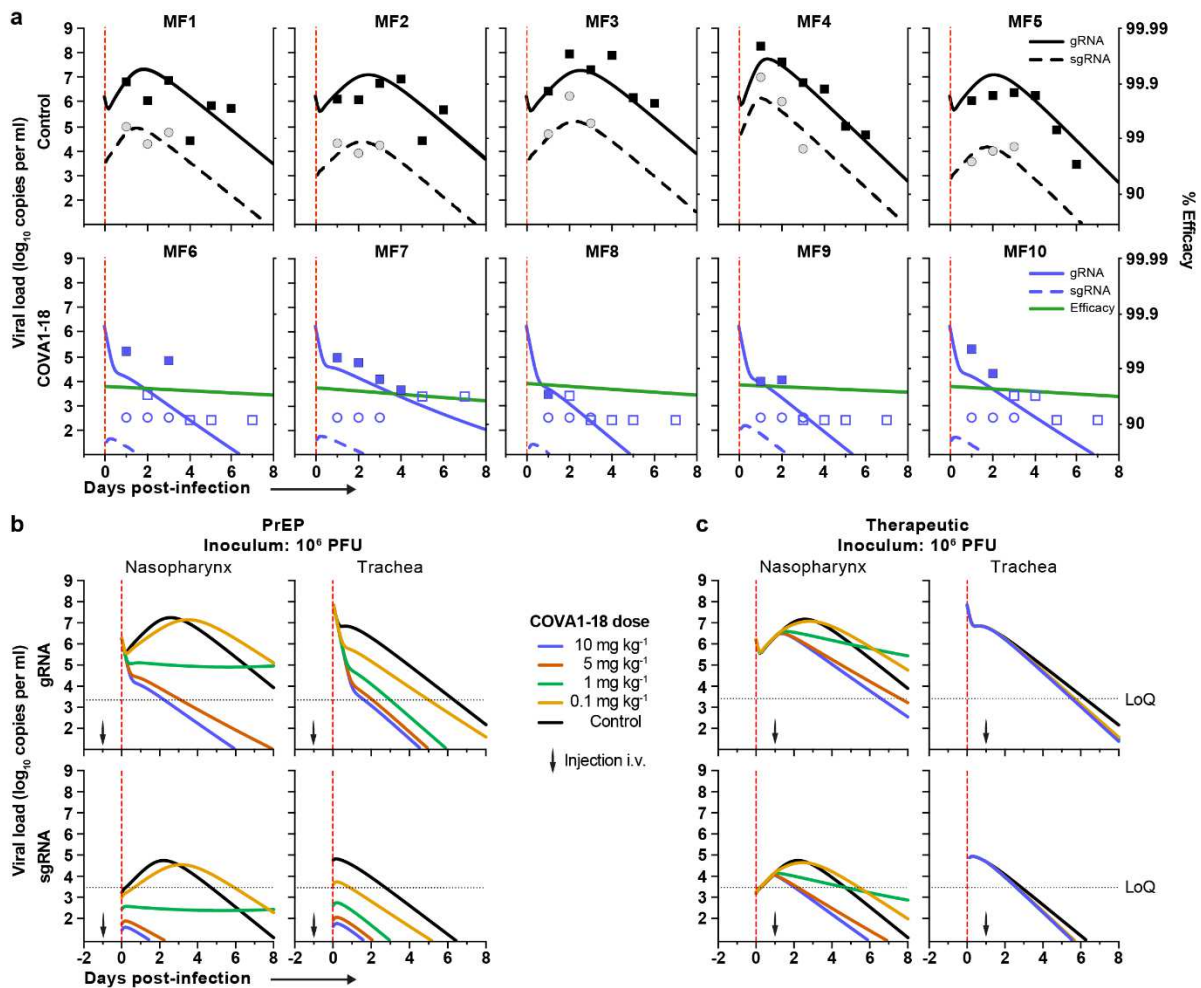
666

667

668

669

Figure 3. COVA1-18 pre-exposure prophylaxis protects cynomolgus monkeys against SARS-CoV-2 challenge and clinical symptoms. (a) Genomic (g)RNA and (b) subgenomic (sg)RNA loads determined by PCR in nasopharyngeal fluids (left), tracheal fluids (middle) and bronchoalveolar lavages (BAL) (right). Medians with range are indicated for fluids and bars represent medians for BAL. (c) Chest CT scores were determined at 3 d.p.i. and at 2 or 5 d.p.i. for historical controls. (d) Absolute lymphocyte count in the blood (mean with range). Mann-Whitney unpaired t-test, p values: * < 0.05, ** < 0.01. Ctl., control group; LoD, limit of detection; LoQ, limit of quantification.



670

671

672

673

674

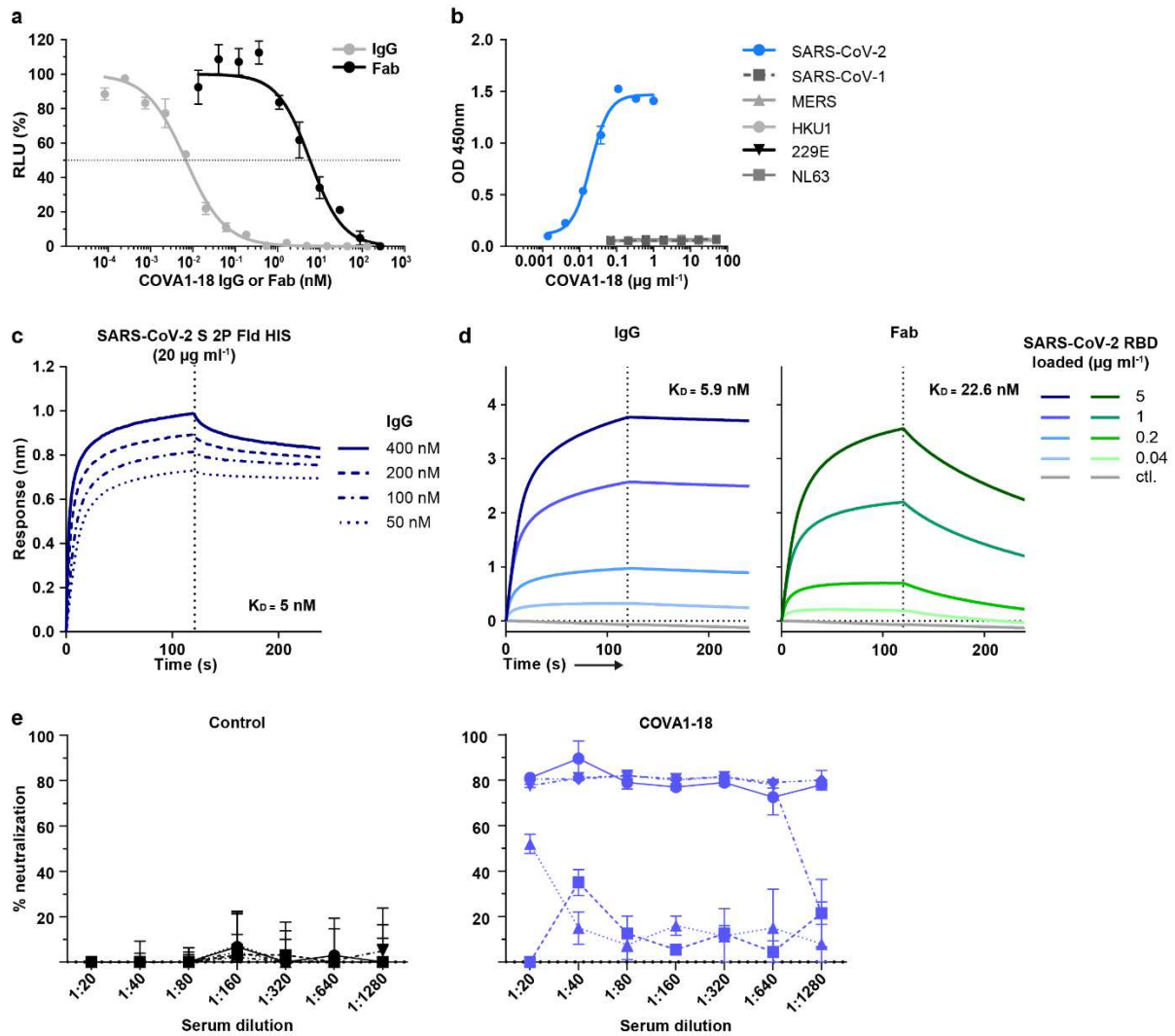
675

676

677

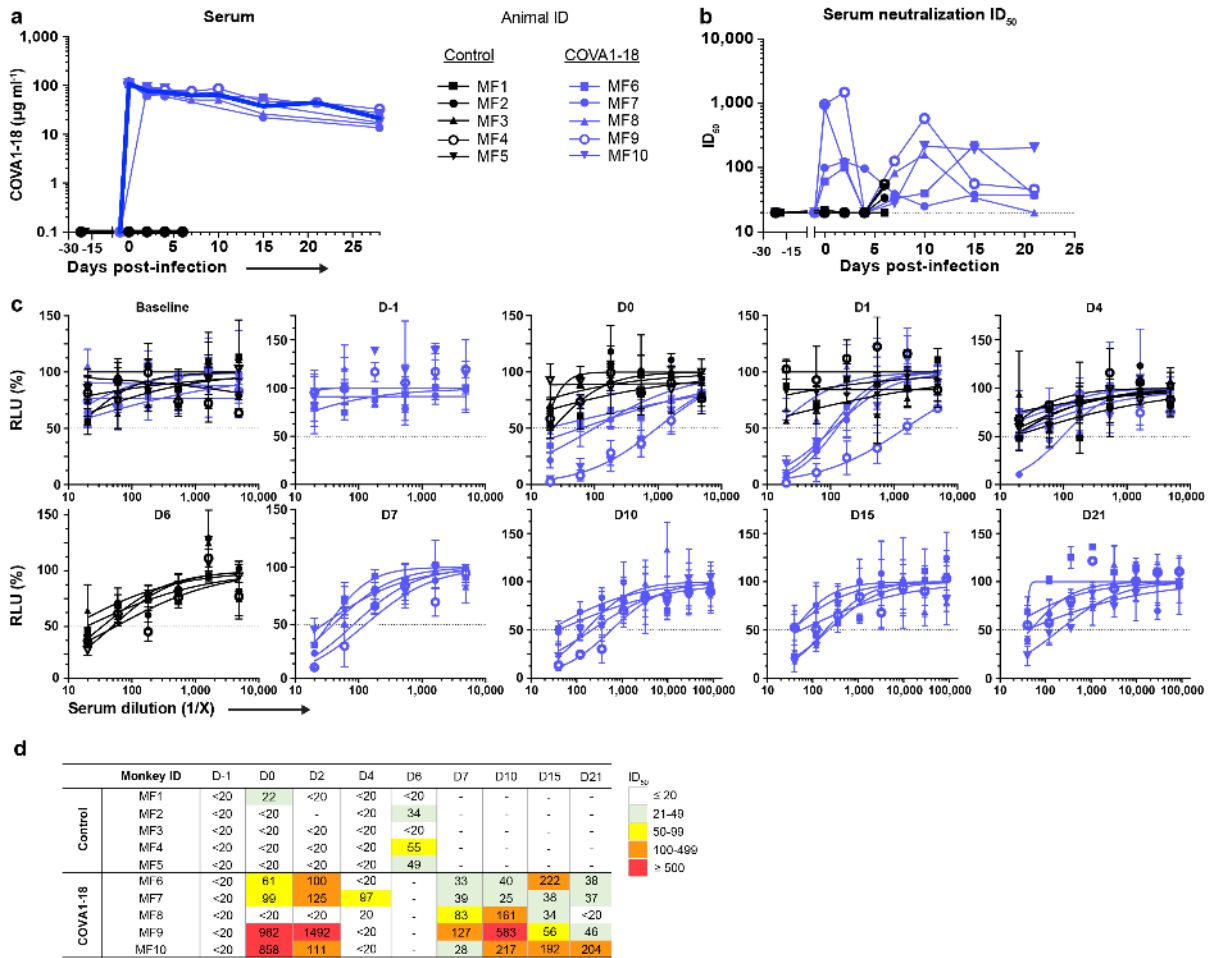
678

Figure 4. Modeling of viral dynamics and treatment efficacy. (a) Individual prediction of the nasopharyngeal gRNA and sgRNA in control (top) and treated animals (bottom) with individual efficacy prediction indicated (green line). The dashed red line indicates the time of infection. gRNA (squares) and sgRNA (circles) data are indicated as plain (above LoQ) or open (below LoQ). (b) Model predictions of gRNA and sgRNA dynamics with 4 doses of COVA1-18 given 24 h prior to challenge (arrow). (c) Simulation as in (b) with COVA1-18 given 24 h post-infection. Black dotted lines indicate LoQ (limit of quantification); i.v., intravenous; PFU, plaque forming units.



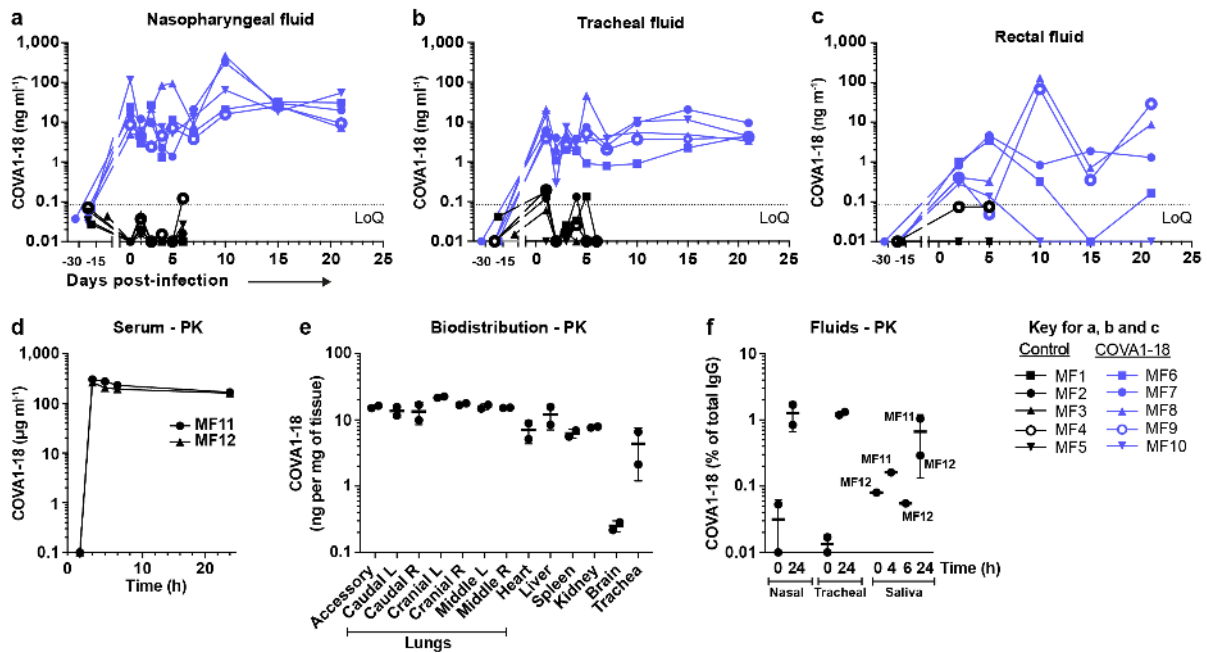
679
680
681
682
683
684
685
686
687
688
689

Extended Data Figure 1. COVA1-18 IgG and Fab neutralization, cross-reactivity, binding kinetic and Syrian hamster serum neutralization. (a) IgG (grey) and Fab (black) pseudotype particle neutralization curves for COVA1-18. Representative of $n \geq 4$ independent experiments. (b) Antigen specificity of COVA1-18 was assessed by ELISA against the soluble S protein derived from different human coronaviruses. (c) BLI sensorgrams of COVA1-18 binding to immobilized soluble SARS-CoV-2 S protein. Representative of $n \geq 2$ independent experiments. (d) BLI sensorgrams of COVA1-18 binding to SARS-CoV-2 RBD loaded onto the sensor chip at various concentrations ($n = 1$). (e) Serum neutralization potency at 3 d.p.i. in Syrian hamsters for the control group (left) and COVA1-18 treated group ($n = 5$ animals per group).



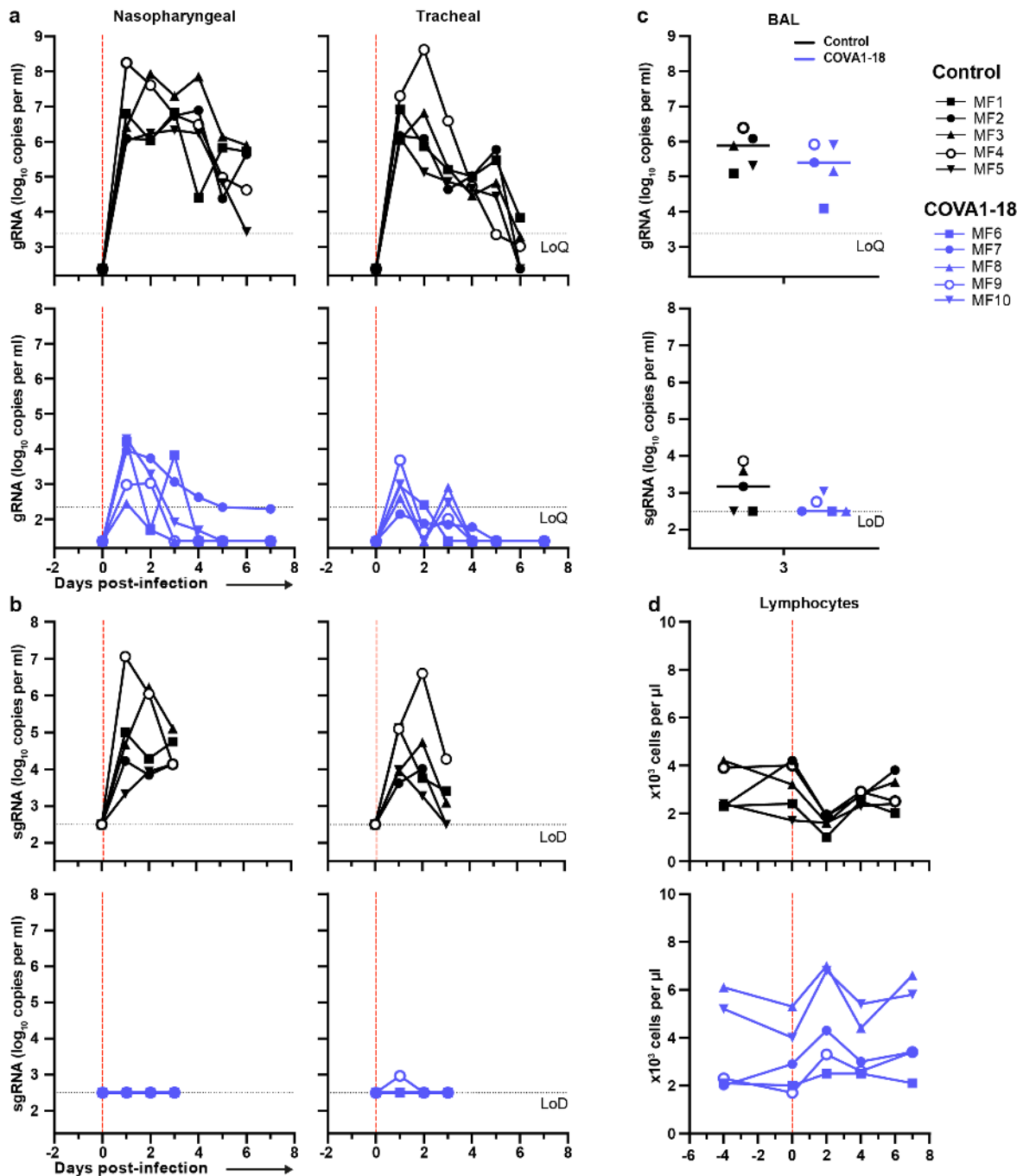
690
691
692
693
694
695
696

Extended Data Figure 2. Serum and mucosal pharmacokinetics of COVA1-18 in treated macaques (1/2). (a) Serum COVA1-18 concentration for each animal. The mean COVA-18 concentration for each group is indicated by a thick blue line (treated animals) and a thick black line (control). (b) Individual serum neutralization ID₅₀. (c) Serum neutralization curve for each animal at the indicated day post-treatment. (d) Individual serum neutralization ID₅₀ with titer range indicated as ID₅₀ 21-49 in green, 50-99 in yellow, 100-499 in orange, >500 red.



697
 698
 699
 700
 701
 702
 703
 704
 705
 706

Extended Data Figure 3. Serum and mucosal pharmacokinetics of COVA1-18 in treated macaques (2/2). The COVA1-18 concentrations measured in nasopharyngeal (a), tracheal (b) and rectal (c) fluids by ELISA are reported for each animal in both groups. (d) Serum COVA1-18 concentration from two animals injected with 10 mg kg^{-1} of COVA1-18 and sampled at 0, 2, 4, 6 and 24 h for a pharmacokinetic (PK) study. (e) The two macaques were euthanized at 24 h post-treatment and organs analyzed to assess the biodistribution of COVA1-18. The concentration of COVA1-18 was normalized to the weight of each sample for every organ. (f) COVA1-18 was measured in fluid samples of the PK study animals and normalized to the total cynomolgus IgG content for each sample. LoQ, limit of quantification.



707

708

709

710

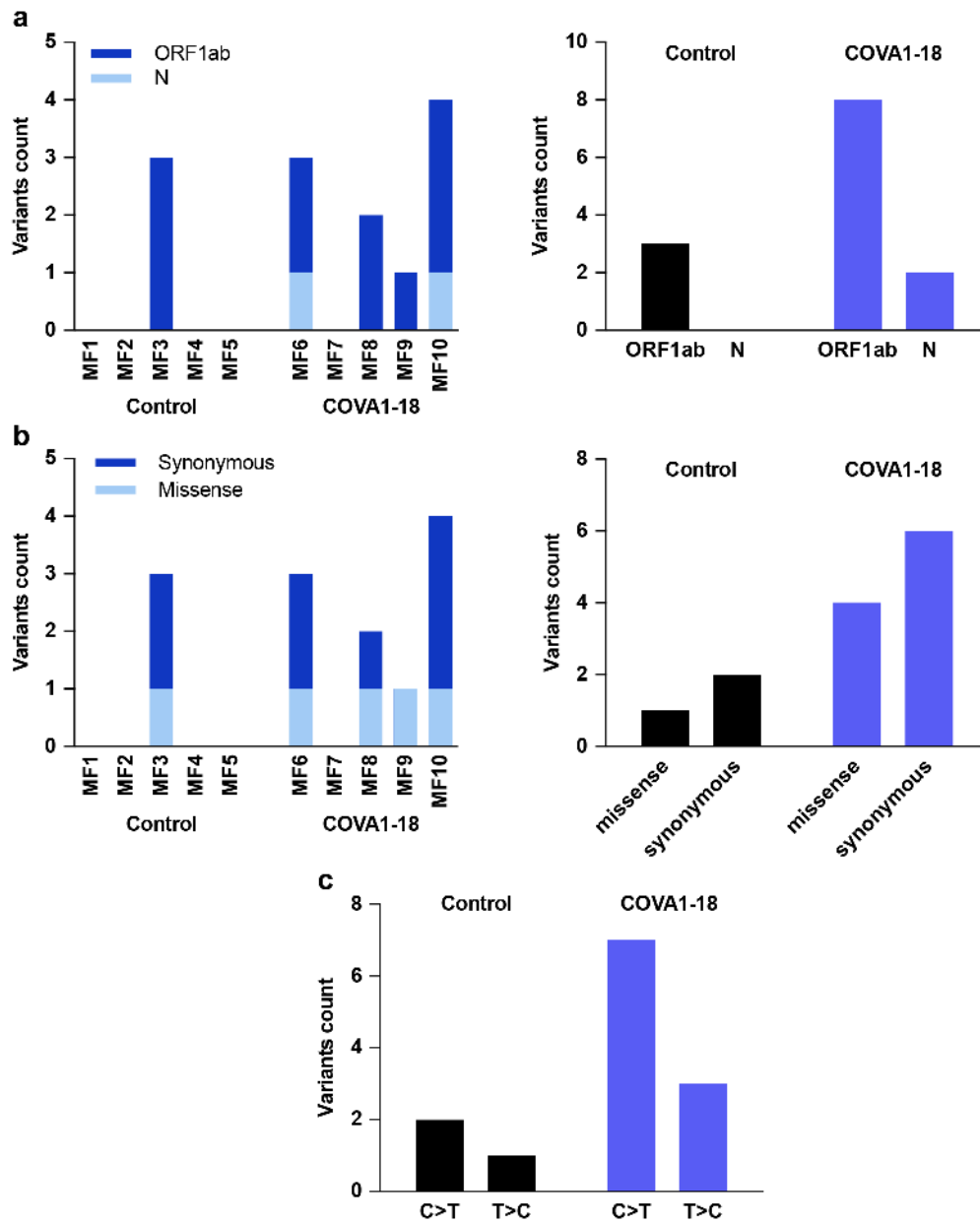
711

712

713

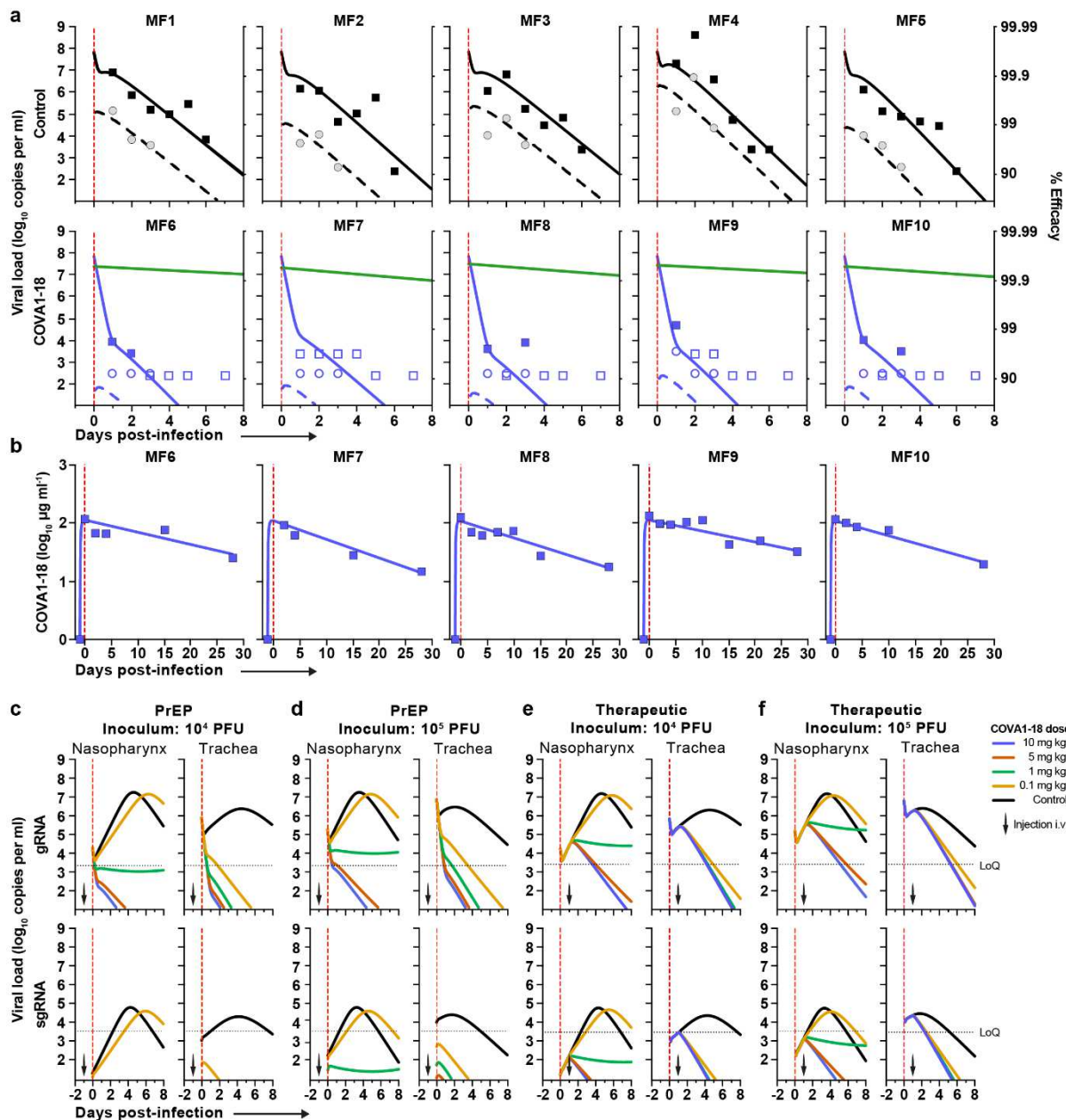
714

Extended Data Figure 4. COVA1-18 pre-exposure prophylaxis protects cynomolgus monkeys against SARS-CoV-2 challenge and clinical symptoms. (a) Genomic (g)RNA and **(b)** subgenomic (sg)RNA loads determined by PCR in nasopharyngeal fluids (left) and tracheal fluids (right) of control (top) and treated (bottom) animals. **(c)** gRNA (top) and sgRNA (bottom) in the bronchoalveolar lavages (BAL) at day 3 post-infection. **(d)** Absolute lymphocyte count in the blood of control (top) and treated (bottom) animals. LoD, limit of detection; LoQ, limit of quantification.



715
716
717
718
719
720
721

Extended Data Figure 5. Sequences in treated and exposed NHP. Viral population sequences in the nasopharyngeal swabs at day 3 were analyzed by Next Generation Sequencing. **(a)** Variants count detected in the N and ORF1ab genes for each individual (left) and cumulative variants count for each gene in the control and COVA1-18 treated groups (right). **(b)** Individual (left) and cumulative (right) synonymous and missense variants count for the control and treated groups. **(c)** Nucleotide substitution observed by type for both groups.



722

723

724

725

726

727

728

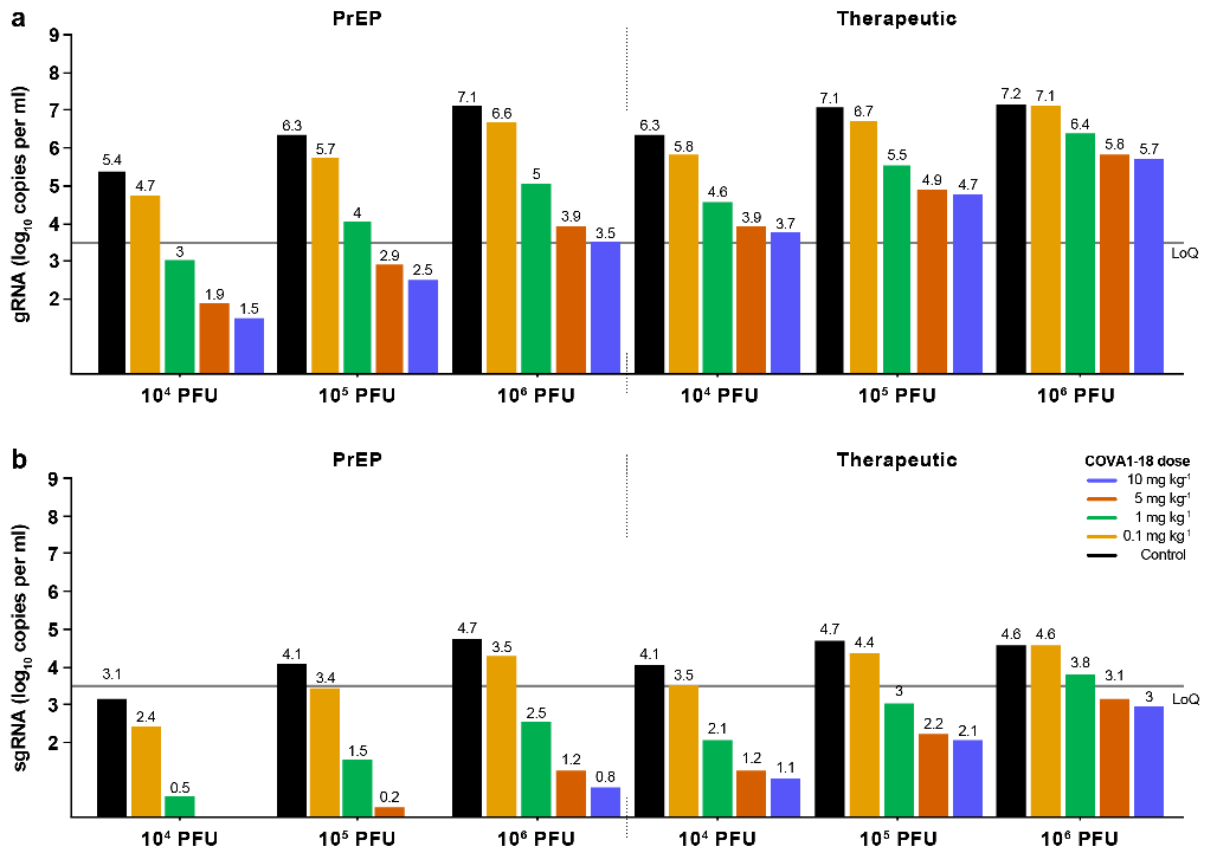
729

730

731

732

Extended Data Figure 6. Modeling of viral dynamics and treatment efficacy (1/2). (a) Individual prediction of the tracheal gRNA and sgRNA in control (top) and treated animals (bottom) with individual efficacy prediction indicated (green line). The dashed red line indicates the time of viral infection. gRNA (squares) and sgRNA (circles) data are indicated as plain (above LoQ) or open (below LoQ). (b) Individual prediction of the COVA1-18 plasma concentration. (c-d) Simulation of the predicted gRNA (top) and sgRNA (bottom) viral loads in the nasopharynx and trachea for a 10^4 and 10^5 PFU challenge dose according to the dose of COVA1-18 given 24 h prior challenge (arrow). (e-f) Simulation as in (c) with COVA1-18 given 24 h post-infection. Black dotted lines indicate the limit of quantification (LoQ). i.v., intravenous; PFU, plaque forming units. PrEP, Pre-Exposure Prophylaxis.



733
734
735
736
737
738
739

Extended Data Figure 7. Modeling of viral dynamics and treatment efficacy (2/2). Simulation of the predicted gRNA (top) and sgRNA (bottom) viral loads in the nasopharynx, according to the dose of COVA1-18 received and the dose of virus received. Left: Pre-Exposure Prophylaxis (PrEP) treatment at -1 d.p.i., viral load measured at 2 d.p.i.; Right: Therapeutic treatment at 1 d.p.i., viral load measured at 3 d.p.i. Black: control; yellow: 0.1 mg kg⁻¹; green: 1 mg kg⁻¹; orange: 5 mg kg⁻¹; blue: 10 mg kg⁻¹. LoQ, limit of quantification.

740 **Extended Data Table 1. BLI and neutralization potency of IgG vs Fab in HEK293T**
 741 **hACE2 cells.** AMC and Duke neutralization assays use lentiviral pseudotyped particles and
 742 HEK293T hACE2 cells. Nexelis neutralization assay uses VSVΔG pseudotyped particles and
 743 Vero E6 cells. BLI, biolayer interferometry; RBD, receptor binding domain.

744

		IC ₅₀				BLI						
		AMC (n ≥ 4)		Duke (n = 1)	Duke D614G (n = 1)	Nexelis (n = 1)	RBD loaded (n = 3)			Soluble S loaded (n = 3)		
		ng ml ⁻¹	pM	ng ml ⁻¹			K _D (nM)	K _a (M ⁻¹ s ⁻¹)	K _d (s ⁻¹)	K _D (nM)	K _a (M ⁻¹ s ⁻¹)	K _d (s ⁻¹)
1-18	IgG	0.8	5.6	9.0	7.0	9.0	7.0	1.7E+05	1.3E-03	5.0	3.7E+05	1.9E-03
	Fab	199.0	3968.0	N/A	N/A	N/A	84.1	5.0E+04	4.1E-03	N/A	N/A	N/A

745 **Extended Data Table 2. Parameter estimates of the viral dynamic model.** RSE: relative
 746 standard error

Parameters	Unit	Description	Fixed effect (RSE%)	Sd of random effect (RSE%)
β_N	ml per copies per day	Virion infectivity	2.14×10^{-4}	0.378
β_T	ml per copies per day		1.68×10^{-3}	
p_N	copies d ⁻¹	Viral production	3.32×10^4	0.552 (99.3)
p_T	copies d ⁻¹		1.12×10^4	
f		Scaling factor for the subgenomic RNA	6.98 (66.7)	1.53 (36)
EC_{50N}	$\mu\text{g ml}^{-1}$	Concentration required to block infectivity by 50%	2.2	0.366 (133)
EC_{50T}	$\mu\text{g ml}^{-1}$		0.053	
EC_{90N}	$\mu\text{g ml}^{-1}$	Concentration required to block infectivity by 90%	19.8	
EC_{90T}	$\mu\text{g ml}^{-1}$		0.48	
δ	d ⁻¹	Baseline clearance rate of productively infected cells	1.88	0.172
ka	d ⁻¹	Absorption rate	4.45	
k	d ⁻¹	Elimination rate	0.0549 (13.3)	0.225 (44.5)
V	ml kg ⁻¹	Volume of distribution	88.7 (6.56)	
D	mg kg ⁻¹	Administered dose of COVA1-18	10	

747

748 **Extended Data Table 3. Mean individual efficacy of the COVA1-18 for each individual in**
749 **both compartments (calculated over the first 10 days of administration).**
750

		MF6	MF7	MF8	MF9	MF10
Mean efficacy (%)	Nasopharynx	97.34	96.67	97.37	97.50	97.16
	Trachea	99.93	99.91	99.93	99.94	99.93

751

752 **Acknowledgments:** We thank Benoit Delache, Sébastien Langlois, Joanna Demilly, Quentin
753 Sconosciuti, Maxime Potier, Nina Dhooge, Pauline Le Calvez, Jean-Marie Robert, Thierry Prot
754 and Christina Dodan for their help with the macaque experiments; Laetitia Bossevot, Marco
755 Leonec, Laurine Moenne-Loccoz and Julie Morin for the RT-qPCR, and for the preparation of
756 reagents; Blanche Fert for her help with the CT scans; Mylinda Barendji, Julien Dinh and
757 Elodie Guyon for the macaque sample processing; Sylvie Keyser for the transports
758 organization; Nastasia Dimant and Brice Targat for their help with the experimental studies in
759 the context of COVID-19-induced constraints; Frédéric Ducancel and Yann Gorin for their
760 help with the logistics and safety management; Isabelle Mangeot for her help with resources
761 management. We thank Sylvie Behillil and Vincent Enouf for contribution to viral stock
762 challenge production, Antoine Nougairède for sharing the plasmid used for the sgRNA assays
763 standardization and Paul Bieniasz for donating cells and reagents for pseudovirus neutralization
764 assays. We thank Matt Hyde and Julie Williams (Animal Resource Center, University of Texas
765 Medical Branch at Galveston) who performed technical procedures with animals. We
766 acknowledge support from CoVIC supported by the Bill and Melinda Gates Foundation. We
767 thank staff at the ISMMS CCMS vivarium for their assistance. We also thank Randy Albrecht
768 for support with the BSL-3 facility and procedures at the ISMMS and Richard Cadagan for
769 excellent technical assistance.

770

771 **Funding:** This study was supported by the Netherlands Organization for Scientific Research
772 (NWO) Vici grant (to R.W.S.), the Bill & Melinda Gates Foundation through the Collaboration
773 for AIDS Vaccine Discovery (CAVD) grant INV-002022 (to R.W.S.), the Fondation Dormeur,
774 Vaduz (to R.W.S. and to M.J.v.G.) and Health Holland PPS-allowance LSHM20040 (to
775 M.J.v.G.). M.J.v.G. is a recipient of an AMC Fellowship, Amsterdam UMC and a COVID-19
776 grant of the Amsterdam Institute of Infection and Immunity, the Netherlands. R.W.S and
777 M.J.v.G. are recipients of support from the University of Amsterdam Proof of Concept fund
778 (contract no 200421) as managed by Innovation Exchange Amsterdam (IXA). The Infectious
779 Disease Models and Innovative Therapies (IDMIT) research infrastructure is supported by the
780 'Programme Investissements d'Avenir, managed by the ANR under reference ANR-11-INBS-
781 0008. The Fondation Bettencourt Schueller and the Region Ile-de-France contributed to the
782 implementation of IDMIT's facilities and imaging technologies. The NHP study received
783 financial support from REACTing, the Fondation pour la Recherche Médicale (FRM, France;
784 AM-CoV-Path) and the European Infrastructure TRANSVAC2 (730964). Work performed at

785 Duke University was supported by the CoVPN grant (NIH AI46705) (to D.C.M.). The Ad5-
786 hACE2 mouse work was supported in part by NIAID R21AI157606 (L.C.), and was partially
787 supported by CRIP (Center for Research for Influenza Pathogenesis), a NIAID supported
788 Center of Excellence for Influenza Research and Surveillance (CEIRS, contract #
789 HHSN272201400008C) (A.G.S.), by supplements to NIAID grant U19AI135972 and DoD
790 grant W81XWH-20-1-0270, by the Defense Advanced Research Projects Agency (HR0011-
791 19-2-0020), and by the generous support of the JPB Foundation, the Open Philanthropy Project
792 (research grant 2020-215611 (5384) and anonymous donors to A.G.S. Part of this study was
793 supported by the Bill and Melinda Gates Foundation through grants OPP1170236 and INV-
794 004923 (I.A.W.) and through the Global Health Vaccine Accelerator Platforms (GH-VAP) and
795 the Coronavirus Immunotherapy Consortium (CoVIC) (Nexelis). The funders had no role in
796 study design, data collection, data analysis, data interpretation, or data reporting.

797

798 **Author contributions:**

799 P.M. and Y.A. conceived, designed, performed experiments, analysed data, managed the
800 project and wrote the manuscript (original draft). A.M. conceived and developed the predictive
801 model, and wrote the manuscript. R.M., N.D.B. performed, supervised and analysed macaque
802 experiments. N.A.K. designed, performed and analysed the hamster experiment. M.S.
803 designed, performed and analysed the mouse experiment. A.W.F. performed the mouse
804 experiment. J.L.S. produced antibodies and performed ELISAs. A.G. contributed to the
805 predictive model development. J.A.B., M.P., C.M., M.O.T., N.S.A. and L.G. performed
806 neutralization assays. V.Ch., S.D. and A.I. performed sequencing, analysed and interpreted the
807 data. A.J.R. analysed the hamster histology data. S.J. and R.R. performed the mouse
808 experiment. T.G.C., P.J.M.B., T.P.L.B., J.v.S., M.B., M.J.v.B., H.L. and M.Y. produced
809 proteins. C.E.M. contributed to the hamster experiment. V.Co. contributed to performing and
810 supervising macaque studies. T.N. and J.L. contributed to the macaque experiments and
811 analysis. N.K. and F.R. contributed to the macaque experiment. C.C. and R.H.T.F. provided
812 resources and supervision for the macaque studies contributed to the macaque experiments and
813 analysis. D.C.M., I.A.W., G.J.d.B. and A.G.S. provided resources and funding. E.G. provided
814 resources and supervision for the sequencing. L.C. conceived, designed and performed the
815 mouse study; acquired funding. A.B. designed and supervised the hamster study, provided
816 funding. S.V.D.W. provided the virus for the macaque study; J.G. conceived and developed
817 the predictive model, supervised, provided funding and wrote the manuscript. M.J.v.G, R.L.G
818 and R.W.S. conceived, designed, supervised the project, acquired funding, provided resources

819 and wrote the manuscript. All authors contributed to the review and editing of the final
820 manuscript.

821

822 **Competing interests:**

823 Amsterdam UMC filed a patent application on SARS-CoV-2 monoclonal antibody COVA1-
824 18. The García-Sastre Laboratory has received research support from Pfizer, Senhwa
825 Biosciences, 7Hills Pharma, Pharmamar, Blade Therapeutics, Avimex, Johnson & Johnson,
826 Dynavax, Manufacturing ImmunityBio and Nanocomposix. Adolfo García-Sastre has
827 consulting agreements for the following companies involving cash and/or stock: Vivaldi
828 Biosciences, Contrafect, 7Hills Pharma, Avimex, Vaxalto, Accurius and Esperovax.

829

830 **Additional information:**

831 Supplementary information is available for this paper.

832 The data that support the findings of this study are available from the corresponding author
833 upon reasonable request.

834 Correspondence and requests for materials should be addressed to roger.le-grand@cea.fr
835 (R.L.G), m.j.vangils@amsterdamumc.nl (M.J.v.G.), r.w.sanders@amsterdamumc.nl (R.W.S.)

836

Figures

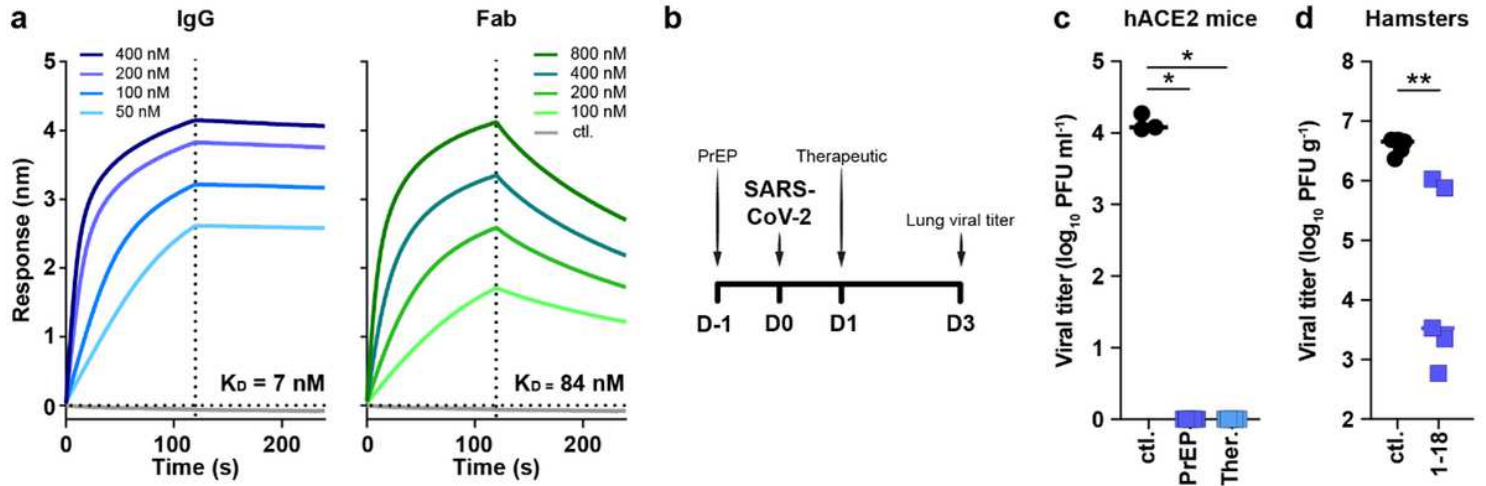


Figure 1

COVA1-18 avidity and SARS-CoV-2 protection in rodents. (a) Bi-layer interferometry sensorgrams comparing COVA1-18 IgG and Fab binding to RBD. K_D s are indicated. Representative of 3 independent experiments. (b) Study design with $n = 5$ per group, except mouse control group ($n = 3$). Hamsters were infected with 105 PFU on day 0 and treated on day 1. Mice received COVA1-18 24 h prior to or after exposure to 104 PFU. Lung viral titers at 3 d.p.i. are shown for mice (c) and hamsters (d). Bars indicate medians. Mann-Whitney unpaired t-test, p values: $* < 0.05$, $** < 0.01$. Ctl., control group; PrEP, pre-exposure prophylaxis; Ther., therapeutic.

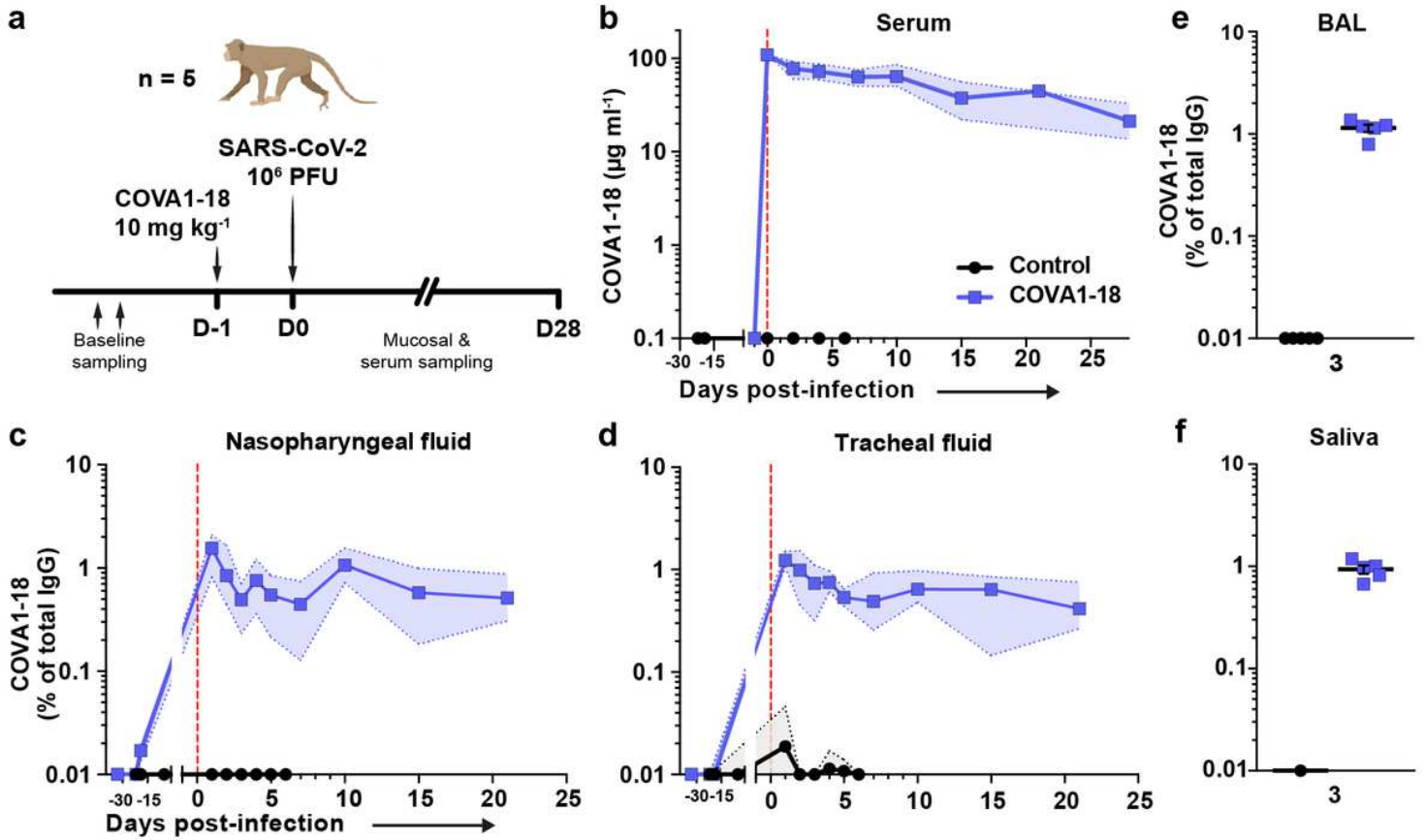


Figure 2

COVA1-18 serum and mucosal pharmacokinetic in infected cynomolgus macaques. (a) Study design. Two groups of n = 5 were exposed to 10⁶ PFU of SARS-CoV-2 (intranasal and intratracheal routes). Treated animals received 10 mg kg⁻¹ of COVA1-18 1 day before challenge. (b) COVA1-18 serum concentration (mean with range). COVA1-18 concentration reported as percent of total cynomolgus IgG in heat-inactivated (c) nasopharyngeal fluid, (d) tracheal fluid (means with range), (e) bronchoalveolar lavage (BAL) and (f) saliva (means ± SEMs). The red dashed line indicates challenge day.

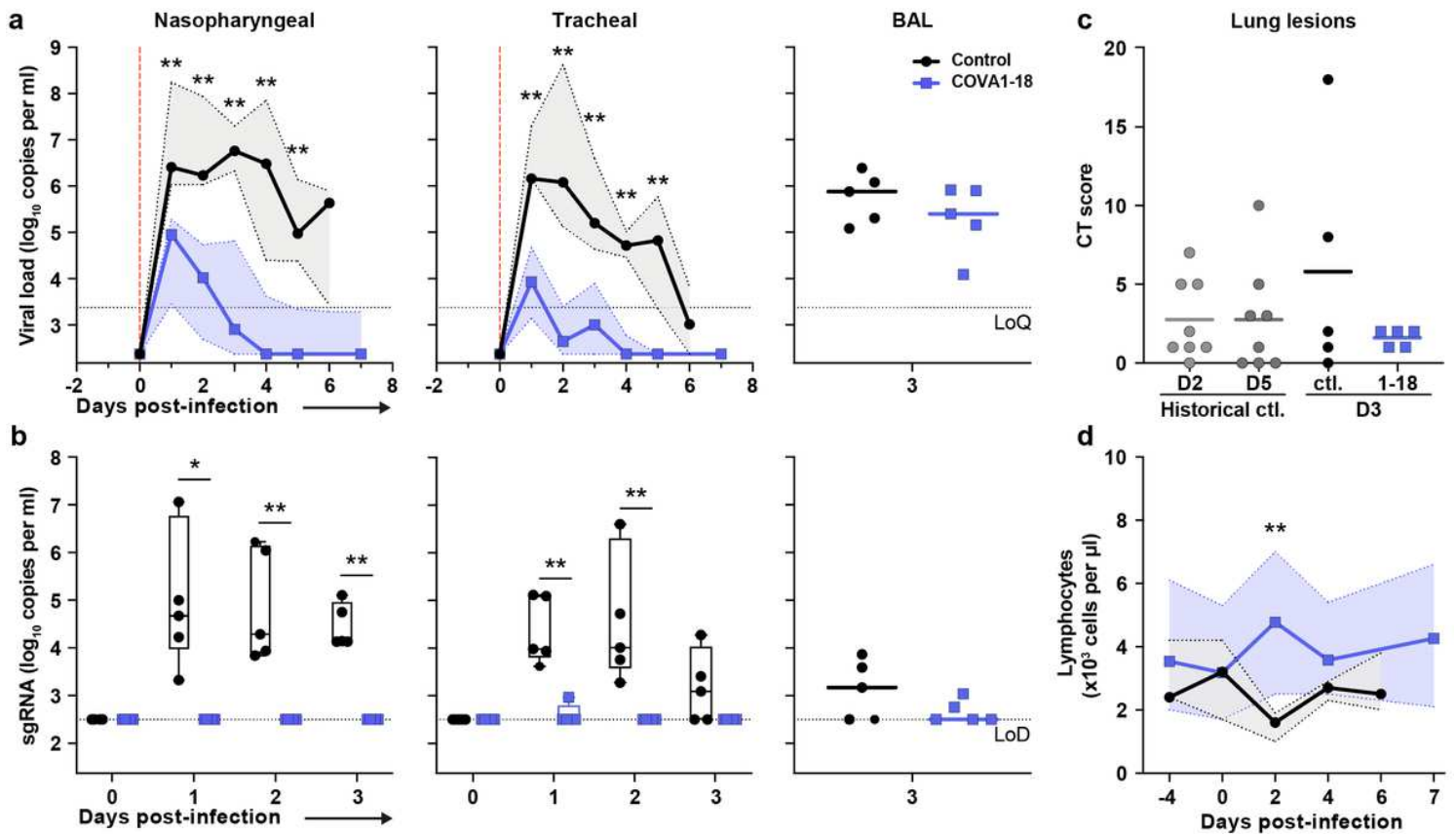


Figure 3

COVA1-18 pre-exposure prophylaxis protects cynomolgus monkeys against SARS-CoV-2 challenge and clinical symptoms. (a) Genomic (g)RNA and (b) subgenomic (sg)RNA loads determined by PCR in nasopharyngeal fluids (left), tracheal fluids (middle) and bronchoalveolar lavages (BAL) (right). Medians with range are indicated for fluids and bars represent medians for BAL. (c) Chest CT scores were determined at 3 d.p.i. and at 2 or 5 d.p.i for historical controls. (d) Absolute lymphocyte count in the blood (mean with range). Mann-Whitney unpaired t-test, p values: * < 0.05, ** < 0.01. Ctl., control group; LoD, limit of detection; LoQ, limit of quantification.

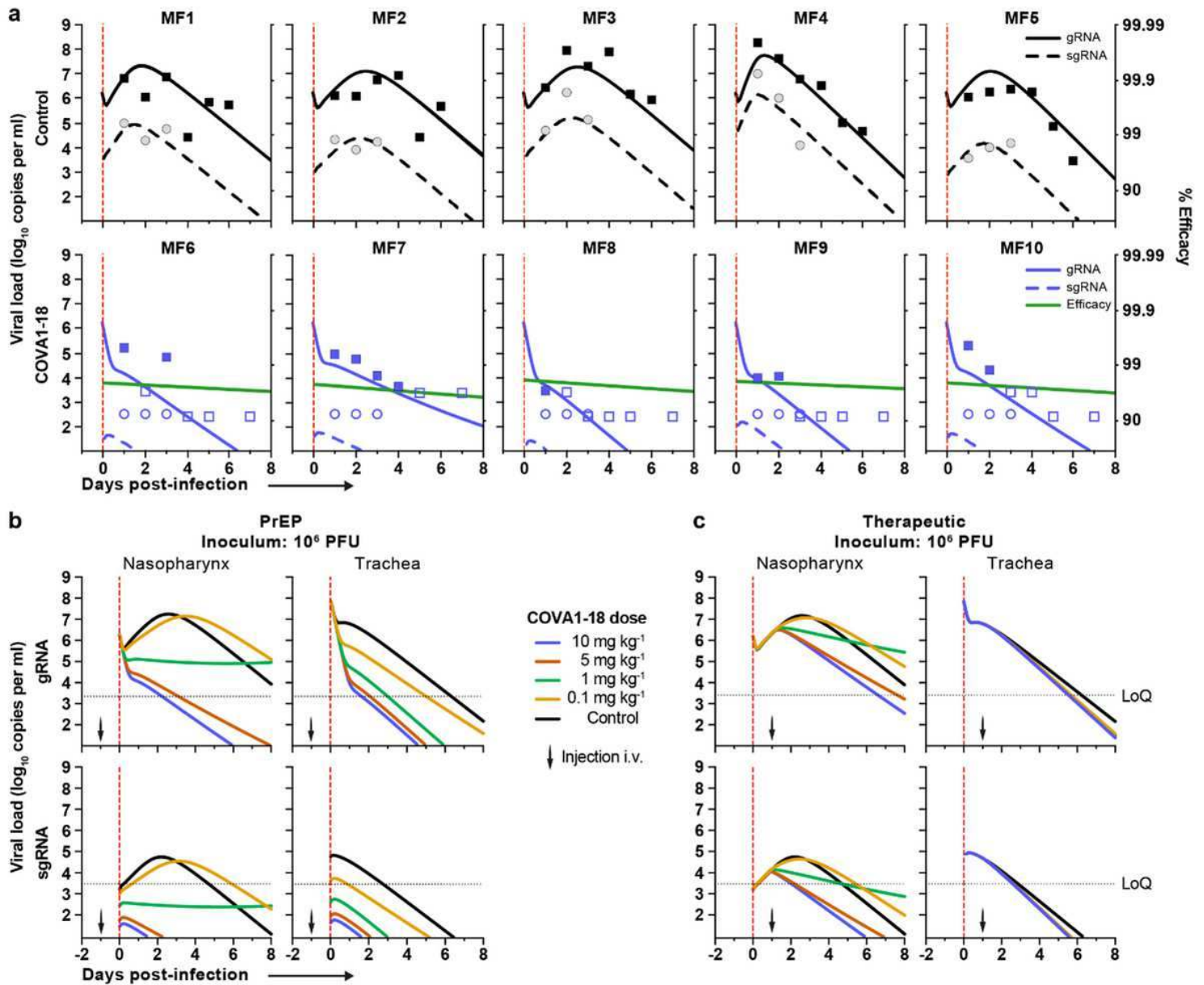


Figure 4

Modeling of viral dynamics and treatment efficacy. (a) Individual prediction of the nasopharyngeal gRNA and sgRNA in control (top) and treated animals (bottom) with individual efficacy prediction indicated (green line). The dashed red line indicates the time of infection. gRNA (squares) and sgRNA (circles) data are indicated as plain (above LoQ) or open (below LoQ). (b) Model predictions of gRNA and sgRNA dynamics with 4 doses of COVA1-18 given 24 h prior to challenge (arrow). (c) Simulation as in (b) with COVA1-18 given 24 h post-infection. Black dotted lines indicate LoQ (limit of quantification); i.v., intravenous; PFU, plaque forming units.

Supplementary Files

This is a list of supplementary files associated with this preprint. Click to download.

- [si.docx](#)